American Mineralogist, Volume 80, pages 502–519, 1995

Thermodynamics of the amphiboles: Fe-Mg cummingtonite solid solutions

Mark S. Ghiorso, Bernard W. Evans
Department of Geological Sciences, AJ-20, University of Washington, Seattle, Washington 98195, U.S.A.
Marc M. Hirschmann
Division of Geological and Planetary Sciences, 170-25, California Institute of Technology, Pasadena, California 91125, U.S.A.
Hexiong Yang
Department of Geological Sciences, AJ-20, University of Washington, Seattle, Washington 98195, U.S.A.

Abstract

A thermodynamic solution model for the ferromagnesian amphiboles is developed. The model accounts explicitly for intersite nonconvergent cation ordering of Fe^{2+} and Mg between octahedral M1, M2, M3, and M4 sites and intrasite interaction energies arising from size-mismatch of unlike cations. The model is formulated with 15 parameters: two standard-state contributions, three ordering energies involving the exchange of Fe^{2+} and Mg between the four crystallographically distinct sites, six reciprocal terms that describe the noncoplanarity of the Gibbs energy of mechanical mixing in composition-ordering space, and four regular-solution type parameters involving Fe^{2+}-Mg interaction on each site. The model may be readily collapsed to approximations that distinguish cation ordering over only three sites (M13, M2, and M4) or two sites (M123 and M4), or that assume the absence of ordering (i.e., a macroscopic model), in which case the number of parameters decreases to 10, 6, and 3, respectively. The proposed model is calibrated for the ferromagnesian monoclinic amphiboles, under the assumptions of energetic equivalency of the M1 and M3 sites and the absence of excess volume or excess vibrational entropy, using the X-ray site occupancy data of Hirschmann et al. (1994) and the phase equilibrium data of Fonarev and Korolkov (1980). Reference-state thermodynamic quantities for magnesio-cummingtonite [$Mg_7Si_8O_{22}(OH)_2$] and grunerite [$Fe_7Si_8O_{22}(OH)_2$] are derived from previously published results. The calibrated model is internally consistent with the database of Berman (1988) and the work of Sack and Ghiorso (1989) on ferromagnesian orthopyroxene. Gibbs energy of mixing, enthalpy of mixing, and activity-composition relation plots are constructed from the calibration.

Introduction

Amphiboles are critical petrogenetic indicators in igneous and metamorphic systems. They have been utilized as temperature, pressure, and reaction-rate sensors for a broad range of P-T conditions, and amphibole-bearing assemblages have found application as a means of estimating the f_{H_2O} and, indirectly, the fluid composition present under the conditions of rock formation. As candidates for thermodynamic models of solid-solution energetics, the amphiboles pose a formidable but fascinating challenge. They are multisite reciprocal solutions that exhibit a high degree of coupled substitution and form solid-solution series with wide compositional variation. Despite this apparent complexity, the petrologic importance of the amphiboles encourages attempts toward a comprehensive thermodynamic formulation. In this paper, we take a first step toward this goal with the formulation and calibration of a thermodynamic model for the monoclinic ferromagnesian amphibole solid solutions (cummingtonite-grunerite series). The reasons for starting with this compositionally simple subsystem are twofold: (1) only Fe^{2+}-Mg cation ordering on octahedral sites is operative because there are no major coupled substitutions and no tetrahedral site ordering, and (2) natural parageneses exist to which the resulting thermodynamic formulation can be applied directly.

The thermodynamic model proposed here is based upon our experience with other ferromagnesian silicates (Sack and Ghiorso, 1989, 1994a, 1994b, 1994c; Hirschmann, 1991) and oxide minerals (Ghiorso, 1990a; Sack and Ghiorso 1991a, 1991b; Ghiorso and Sack, 1991). Although the amphiboles are structurally more complex, our approach to construction of the model is in principle identical. We propose a model that accounts explicitly for: (1) the temperature dependence of cation ordering of Fe^{2+} and Mg^{2+} over available crystallographic sites, and (2) the excess enthalpy associated with size-mismatch substitution of Fe^{2+} and Mg^{2+} on individual sites. We demonstrate that, as is the case for all mineral solid solutions that exhibit cation ordering, calibration of this model requires three diverse datasets: (1) information on

0003–004X/95/0506–0502$02.00

the thermodynamic properties of end-member (standard-state) compositions, (2) the temperature and compositional dependence of cation ordering, and (3) the compositions of ferromagnesian amphibole coexisting with other mineral phases in Fe^{2+}-Mg exchange equilibrium. Fortunately, experimental data for the ferromagnesian amphiboles adequately constrain the end-member properties, and recent experimental and analytical work (Hirschmann et al., 1994) documents the temperature and compositional dependence of cation ordering. These data, when combined with experimental constraints on the stability of cummingtonite solid solutions coexisting with orthopyroxene, H_2O, and quartz, allow calibration of the parameters of the model. Our model incorporates new experimental data and represents a major revision of attempts to determine the solution properties of the cummingtonite series made over the last three decades (Mueller, 1961, 1962; Saxena, 1973; Fonarev, 1981; Ganguly, 1982).

Thermodynamic formulation

Our philosophical approach in formulating a thermodynamic model for the Fe-Mg cummingtonite solid solutions is to construct a model that is extensible in composition. We intend to use the model proposed here as a base for developing a formulation for the amphibole quadrilateral and, ultimately, for a description of the energetics of aluminous orthoamphibole and hornblende. Subsequent extensions should be additive and not necessitate reformulation or recalibration of the constituent subsystems. For this reason, the formulation proposed here will make allowance for contributions to the energetics of mixing, which may be of minor significance in the (Fe^{2+},Mg) monoclinic series but which must be included in light of the potential contribution to other amphibole solid solutions. Of paramount importance to this issue of extensibility is the formulation of a model that accounts explicitly for the configurational entropy arising from long-range, nonconvergent cation ordering.

Formulation of a four-site, nonconvergent cation-ordering model

In the ferromagnesian amphiboles the Fe^{2+} and Mg^{2+} ions occupy four crystallographically distinct sites, designated M1–M4. The M1, M2, and M3 sites are octahedrally coordinated by apical O atoms of upward and downward pointing, double-chain silicate tetrahedra, whereas the M4 site is coordinated by basal O atoms from adjacent, double-chain "I-beam" units (Hawthorne, 1981). In addition, the M1 and M3 cations are respectively cis- and trans-coordinated with associated monovalent anions. There are two M1, M2, and M4 sites per formula unit [$M_7Si_8O_{22}(OH)_2$, M = Fe^{2+} or Mg^{2+}] and one M3 site. The large and distorted M4 site displays the strongest preference for Fe^{2+} over Mg^{2+}. Mössbauer spectra of a wide range of cummingtonite-grunerite solid solutions (Bancroft et al., 1967; Hafner and Ghose, 1971; Ghose and Weidner, 1972; Barabanov and Tomilov, 1973; Ying et al., 1989) and anthophyllite solid solutions (Seifert and Virgo, 1974; Seifert, 1978; Law, 1989) have been interpreted as though Fe^{2+} and Mg^{2+} were randomly distributed over the remaining M1, M2, and M3 octahedral sites. X-ray studies indicate that this interpretation is incorrect in detail, with Fe^{2+}-Mg^{2+} ordering occurring between the M2 site and the combined monovalent, anion-coordinated M1 + M3 (hereafter M13) sites (Hawthorne, 1983; Hirschmann et al., 1994). There is little evidence for a statistically significant Fe^{2+}-Mg ordering between the M1 and M3 sites (Hirschmann et al., 1994), but this ordering may become important with Al-substitution on the M2 site or halogen substitution on the monovalent anion site. Accordingly, we develop a general four-site formulation that will eventually be applicable to extensions out of the binary.

For the ferromagnesian amphiboles, the axes of composition-ordering space (Thompson, 1969, 1970) may be defined in terms of one composition variable,

$$r = 2X_{Fe} - 1 \tag{1}$$

and three ordering variables,

$$s_1 = X_{Fe}^{M4} - X_{Fe}^{M1} \tag{2a}$$

$$s_2 = X_{Fe}^{M4} - X_{Fe}^{M2} \tag{2b}$$

$$s_3 = X_{Fe}^{M4} - X_{Fe}^{M3} \tag{2c}$$

where X_{Fe} is the mole fraction of the $Fe_7Si_8O_{22}(OH)_2$ component and X_{Fe}^i refers to the mole fraction of Fe on the ith crystallographic site. Definitions of site mole fractions consistent with Equations 1 and 2 are provided in Table 1. We seek a parameterization for the molar Gibbs free energy the solution $\overline{G}$, defined by Thompson (1969, 1970) as

$$\overline{G} = -T\overline{S}_{conf} + \overline{G}^* \tag{3}$$

where $\overline{G}^*$ is the vibrational molar Gibbs free energy of the solution, T is the absolute temperature, and $\overline{S}_{conf}$ is the configurational entropy of mixing. The last may be written as

$$\begin{aligned}\overline{S}_{conf} = -\mathrm{R}(&2X_{Fe}^{M1}\ln X_{Fe}^{M1} + 2X_{Mg}^{M1}\ln X_{Mg}^{M1} + 2X_{Fe}^{M2}\ln X_{Fe}^{M2} \\ &+ 2X_{Mg}^{M2}\ln X_{Mg}^{M2} + X_{Fe}^{M3}\ln X_{Fe}^{M3} + X_{Mg}^{M3}\ln X_{Mg}^{M3} \\ &+ 2X_{Fe}^{M4}\ln X_{Fe}^{M4} + 2X_{Mg}^{M4}\ln X_{Mg}^{M4})\end{aligned} \tag{4}$$

where R is the gas constant. We assume that $\overline{G}^*$ may be expressed as a truncated second-order Taylor expansion in both composition and ordering variables:

$$\begin{aligned}\overline{G}^* = &\overline{G}_0^* + \overline{G}_r^* r + \overline{G}_{s_1}^* s_1 + \overline{G}_{s_2}^* s_2 + \overline{G}_{s_3}^* s_3 + \overline{G}_{r,r}^* r^2 \\ &+ \overline{G}_{r,s_1}^* r s_1 + \overline{G}_{r,s_2}^* r s_2 + \overline{G}_{r,s_3}^* r s_3 + \overline{G}_{s_1,s_1}^* s_1^2 \\ &+ \overline{G}_{s_1,s_2}^* s_1 s_2 + \overline{G}_{s_1,s_3}^* s_1 s_3 + \overline{G}_{s_2,s_2}^* s_2^2 + \overline{G}_{s_2,s_3}^* s_2 s_3 \\ &+ \overline{G}_{s_3,s_3}^* s_3^2\end{aligned} \tag{5}$$

which, as we shall see below, is consistent with the assumption of symmetric regular-solution type interactions

TABLE 1. Definitions of site mole fractions

	Four-site model	Three-site model	Two-site model
r	$^4/_7X^{M1}_{Fe} + {}^4/_7X^{M2}_{Fe} + {}^2/_7X^{M3}_{Fe} + {}^4/_7X^{M4}_{Fe} - 1$	$^6/_7X^{M13}_{Fe} + {}^4/_7X^{M2}_{Fe} + {}^4/_7X^{M4}_{Fe} - 1$	$^{10}/_7X^{M123}_{Fe} + {}^4/_7X^{M4}_{Fe} - 1$
s_1	$X^{M4}_{Fe} - X^{M1}_{Fe}$		
s_2	$X^{M4}_{Fe} - X^{M2}_{Fe}$	$X^{M4}_{Fe} - X^{M2}_{Fe}$	
s_3	$X^{M4}_{Fe} - X^{M3}_{Fe}$		
s_{13}		$X^{M4}_{Fe} - X^{M13}_{Fe}$	
s_{123}			$X^{M4}_{Fe} - X^{M123}_{Fe}$
X^{M1}_{Fe}	$1/2 + 1/2 - {}^5/_7s_1 + {}^2/_7s_2 + {}^1/_7s_3$		
X^{M2}_{Fe}	$1/2 + 1/2 + {}^2/_7s_1 - {}^5/_7s_2 + {}^1/_7s_3$	$1/2 + 1/2 + {}^3/_7s_{13} - {}^5/_7s_2$	
X^{M3}_{Fe}	$1/2 + 1/2 + {}^2/_7s_1 + {}^2/_7s_2 - {}^6/_7s_3$		
X^{M4}_{Fe}	$1/2 + 1/2 + {}^2/_7s_1 + {}^2/_7s_2 + {}^1/_7s_3$	$1/2 + 1/2 + {}^3/_7s_{13} + {}^2/_7s_2$	$1/2 + 1/2 + {}^5/_7s_{123}$
X^{M1}_{Mg}	$1/2 - 1/2 + {}^5/_7s_1 - {}^2/_7s_2 - {}^1/_7s_3$		
X^{M2}_{Mg}	$1/2 - 1/2 - {}^2/_7s_1 + {}^5/_7s_2 - {}^1/_7s_3$	$1/2 - 1/2 - {}^3/_7s_{13} + {}^5/_7s_2$	
X^{M3}_{Mg}	$1/2 - 1/2 - {}^2/_7s_1 - {}^2/_7s_2 + {}^6/_7s_3$		
X^{M4}_{Mg}	$1/2 - 1/2 - {}^2/_7s_1 - {}^2/_7s_2 - {}^1/_7s_3$	$1/2 - 1/2 - {}^3/_7s_{13} - {}^2/_7s_2$	$1/2 - 1/2 - {}^5/_7s_{123}$
X^{M13}_{Fe}		$1/2 + 1/2 - {}^4/_7s_{13} + {}^2/_7s_2$	
X^{M13}_{Mg}		$1/2 - 1/2 + {}^4/_7s_{13} - {}^2/_7s_2$	
X^{M123}_{Fe}			$1/2 + 1/2 - {}^2/_7s_{123}$
X^{M123}_{Mg}			$1/2 - 1/2 + {}^2/_7s_{123}$

Note: $r = 2X_{Fe} - 1$.

between Fe^{2+} and Mg cations on equivalent sites. The Taylor expansion coefficients, $\overline{G}^*_i$, of Equation 5 constitute 15 parameters meant to embody energetic consequences of both standard-state and mixing contributions. In order to see this distinction more clearly, it is convenient to recast the Taylor expansion coefficients into an equivalent, but arguably more intuitive, set of 15 preferred model parameters. There are innumerable ways to effect this transformation, but we will be guided in our selection by a close examination of the topology of $\overline{S}_{conf}$ within composition-ordering space.

$\overline{S}_{conf}$ is a function of r, s_1, s_2, and s_3 (Table 1) and is zero for the end-member compositions $Mg_7Si_8O_{22}(OH)_2$ (Cm) and $Fe_7Si_8O_{22}(OH)_2$ (Gn) and for 14 intermediate compositions possessing cation distributions corresponding to perfectly ordered or antiordered configurations. These nodes of zero $\overline{S}_{conf}$ are referred to as the vertices of composition-ordering space, which we enumerate in Table 2. The Gibbs free energies of the internal nodes may be related to those of the end-members by defining reciprocal exchange reactions, e.g.,

$$Mg_7Si_8O_{22}(OH)_2 + Fe_7Si_8O_{22}(OH)_2 = Fe_2^{M4}Mg_2^{M1}Mg_2^{M2}Mg^{M3}Si_8O_{22}(OH)_2 + Mg_2^{M4}Fe_2^{M1}Fe_2^{M2}Fe^{M3}Si_8O_{22}(OH)_2. \quad (6)$$

The free energy change corresponding to Equation 6 is denoted $\Delta\overline{G}^0_{X,123,4}$. (We adopt a notation for naming reciprocal reactions by designating Fe-occupation of sites in the products; $\Delta\overline{G}^0_{X,123,4}$ refers to the pure Mg and Fe end-members reacting to form one formula unit with Fe on the M1, M2, and M3 sites and Mg on the M4 site, and another with Fe on the M4 site and Mg on the M1, M2, and M3 sites.) A total of seven reactions of this type may be written (Table 3), but only six of these are linearly independent. This is because the reciprocal exchange energies correspond physically to departures from linearity in the mechanical Gibbs energy of mixing defined for each bounding binary of composition-ordering space. As this space is four-dimensional, there are (4·3)/2 binary subsystems and therefore six unique exchange energies. This redundancy can be quantified by computing each of the seven exchange energies in terms of our model parameterization of $\overline{G}(r, s_1, s_2, s_3)$, e.g., by substituting into Equation 5, $\Delta\overline{G}^0_{X,123,4}$ evaluates to:

$$\begin{aligned}\overline{G}(3/7,-1,-1,-1) + \overline{G}(-3/7,1,1,1) - \overline{G}(1,0,0,0) - \overline{G}(-1,0,0,0) \\ = -{}^{80}/_{49}\overline{G}^*_{r,r} - {}^9/_7(\overline{G}^*_{r,s_1} + \overline{G}^*_{r,s_2} + \overline{G}^*_{r,s_3}) \\ + 2(\overline{G}^*_{s_1,s_1} + \overline{G}^*_{s_1,s_2} + \overline{G}^*_{s_1,s_3} + \overline{G}^*_{s_2,s_2} + \overline{G}^*_{s_2,s_3} + \overline{G}^*_{s_3,s_3}).\end{aligned} \quad (7)$$

Examination of these seven expansions reveals the identity $\Delta\overline{G}^0_{X,14,23} + \Delta\overline{G}^0_{X,12,34} + \Delta\overline{G}^0_{X,13,34} = \Delta\overline{G}^0_{X,234,1} + \Delta\overline{G}^0_{X,134,2} + \Delta\overline{G}^0_{X,124,3} + \Delta\overline{G}^0_{X,123,4}$. We choose $\Delta\overline{G}^0_{X,14,23}$ as the dependent parameter.

In addition to the six reciprocal exchange energies, it is logical to add to the list of preferred parameters the Gibbs free energies of the two end-members ($\overline{G}^0_{Cm}$ and $\overline{G}^0_{Gn}$) and four intrasite Fe^{2+}-Mg interaction energies. The latter may be conveniently evaluated in terms of regular-solution-like, symmetric binary interactions associated with unlike cations on a given site. These we denote W_1, W_2, W_3, and W_4 for the M1, M2, M3 and M4 sites, respectively. As an example of their definition, W_4 is related to the vibrational Gibbs energy at the midpoint $(-3/7,1/2,1/2,1/2)$ of the $Mg_7Si_8O_{22}(OH)_2(-1,0,0,0) - Fe_2^{M4}Mg_2^{M1}Mg_2^{M2}Mg^{M3}Si_8O_{22}(OH)_{22}$ $(-3/7,1,1,1)$ join, that is

$$\overline{G}^*(3/7,1/2,1/2,1/2) = 1/2[\overline{G}^*(-3/7,1,1,1) + \overline{G}^*(-1,0,0,0)] + \frac{(2W_4)}{4}. \quad (8)$$

TABLE 2. Vertices of composition-ordering space

r	−1	−5/7	−3/7	−1/7	1/7	3/7	5/7	1
				Four-site formulation				
	MgMgMgMg	MgMgMgFe	FeMgMgMg MgFeMgMg MgMgFeMg	FeMgMgFe MgFeMgFe MgMgFeFe	FeFeMgMg FeMgFeMg MgFeFeMg	FeFeMgFe FeMgFeFe MgFeFeFe	FeFeFeMg	FeFeFeFe
				Three-site formulation				
	MgMgMgMg		FeMgMgMg MgMgFeMg	MgFeMgFe	FeMgFeMg	FeFeMgFe MgFeFeFe		FeFeFeFe
				Two-site formulation				
	MgMgMgMg		FeMgMgMg			MgFeFeFe		FeFeFeFe

Note: MMMM = $M_{\frac{1}{2}}^{M4}M_{\frac{1}{2}}^{M1}M_{\frac{1}{2}}^{M2}M^{M3}Si_8O_{22}(OH)_2$.

The remaining three preferred parameters are defined to correspond to the Gibbs energies of ordering reactions. The stoichiometries of these reactions may be deduced from the conditions of homogeneous (or internal) equilibrium with respect to cation ordering:

$$\frac{\partial \overline{G}}{\partial s_1} = 0 \tag{9a}$$

$$\frac{\partial \overline{G}}{\partial s_2} = 0 \tag{9b}$$

$$\frac{\partial \overline{G}}{\partial s_3} = 0. \tag{9c}$$

For example, upon substitution of Equations 3, 4, and 5, Equation 9a becomes

$$-\overline{G}^*_{s_1} = RT \ln\left[\left(\frac{X^{M1}_{Mg}}{X^{M1}_{Fe}}\right)^{1/8}\left(\frac{X^{M2}_{Fe}}{X^{M2}_{Mg}}\right)^{1/4}\left(\frac{X^{M3}_{Fe}}{X^{M3}_{Mg}}\right)^{3/8}\left(\frac{X^{M4}_{Fe}}{X^{M4}_{Mg}}\right)^{1/2}\right] + \overline{G}^*_{r,s_1} r + 2\overline{G}^*_{s_1,s_1} s_1 + \overline{G}^*_{s_1,s_2} s_2 + \overline{G}^*_{s_1,s_3} s_3. \tag{10}$$

The Taylor coefficient on the left side of this expression is the Gibbs energy of a reaction ($\Delta\overline{G}^0_{ORD,1}$) that coincides with cation redistribution corresponding to the transfer of Fe^{2+} from M1 to the M2, M3, and M4 sites. In terms of the vertices of composition-ordering space, such a reaction is given by the entry for $\Delta\overline{G}^0_{ORD,1}$ provided in Table 3. Equivalent analysis of Equations 9b and 9c provides definitions for the remaining two preferred model parameters, $\Delta\overline{G}^0_{ORD,2}$ and $\Delta\overline{G}^0_{ORD,3}$ (Table 3).

Relations between the Taylor expansion coefficients of Equation 5 and the preferred set of model parameters may be obtained by writing out definitions of each of the parameters (e.g., Eqs. 7 and 8) in terms of the Taylor expansion coefficients. The 15 Taylor expansion coefficients may then be uniquely expressed in terms of the 15 preferred model parameters by solving the set of 15 linear expressions given by these definitions. The result is presented in Table 4. Substitution of these identities into Equation 5 provides our model equation for the molar vibrational Gibbs free energy of ferromagnesian amphiboles. Considerable simplification and insight can be achieved by utilizing definitions from Table 1 and writing this quantity in terms of site mole fractions:

TABLE 3. Reciprocal exchange and reciprocal ordering exchange reactions

Parameter	Reaction $(M4)_2(M1)_2(M2)_2(M3)Si_8O_{22}(OH)_2$
$\Delta\overline{G}^0_{X,234,1}$	$Mg_2Mg_2Mg_2Mg + Fe_2Fe_2Fe_2Fe = Fe_2Mg_2Fe_2Fe + Mg_2Fe_2Mg_2Mg$
$\Delta\overline{G}^0_{X,134,2}$	$Mg_2Mg_2Mg_2Mg + Fe_2Fe_2Fe_2Fe = Fe_2Fe_2Mg_2Fe + Mg_2Mg_2Fe_2Mg$
$\Delta\overline{G}^0_{X,124,3}$	$Mg_2Mg_2Mg_2Mg + Fe_2Fe_2Fe_2Fe = Fe_2Fe_2Fe_2Mg + Mg_2Mg_2Mg_2Fe$
$\Delta\overline{G}^0_{X,123,4}$	$Mg_2Mg_2Mg_2Mg + Fe_2Fe_2Fe_2Fe = Mg_2Fe_2Fe_2Fe + Fe_2Mg_2Mg_2Mg$
$\Delta\overline{G}^0_{X,12,34}$	$Mg_2Mg_2Mg_2Mg + Fe_2Fe_2Fe_2Fe = Mg_2Fe_2Fe_2Mg + Fe_2Mg_2Mg_2Fe$
$\Delta\overline{G}^0_{X,13,24}$	$Mg_2Mg_2Mg_2Mg + Fe_2Fe_2Fe_2Fe = Mg_2Fe_2Mg_2Fe + Fe_2Mg_2Fe_2Mg$
$\Delta\overline{G}^0_{X,14,23}$ (= $\Delta\overline{G}^0_{X,23,14}$)	$Mg_2Mg_2Mg_2Mg + Fe_2Fe_2Fe_2Fe = Fe_2Fe_2Mg_2Mg + Mg_2Mg_2Fe_2Fe$
$\Delta\overline{G}^0_{ORD,1}$	$\frac{1}{8}Fe_2Fe_2Fe_2Mg + \frac{1}{8}Fe_2Fe_2Mg_2Fe + \frac{1}{8}Mg_2Fe_2Fe_2Fe + \frac{3}{8}Mg_2Fe_2Mg_2Mg + \frac{1}{28}Mg_2Mg_2Mg_2Mg = \frac{1}{8}Mg_2Mg_2Mg_2Fe + \frac{1}{8}Mg_2Mg_2Fe_2Mg + \frac{1}{8}Fe_2Mg_2Mg_2Mg + \frac{3}{8}Fe_2Mg_2Fe_2Fe + \frac{1}{28}Fe_2Fe_2Fe_2Fe$
$\Delta\overline{G}^0_{ORD,2}$	$\frac{1}{8}Fe_2Fe_2Fe_2Mg + \frac{1}{8}Fe_2Mg_2Fe_2Fe + \frac{1}{8}Mg_2Fe_2Fe_2Fe + \frac{3}{8}Mg_2Mg_2Fe_2Mg + \frac{1}{28}Mg_2Mg_2Mg_2Mg = \frac{1}{8}Mg_2Mg_2Mg_2Fe + \frac{1}{8}Mg_2Fe_2Mg_2Mg + \frac{1}{8}Fe_2Mg_2Mg_2Mg + \frac{3}{8}Fe_2Fe_2Mg_2Fe + \frac{1}{28}Fe_2Fe_2Fe_2Fe$
$\Delta\overline{G}^0_{ORD,3}$	$\frac{1}{8}Fe_2Mg_2Fe_2Fe + \frac{1}{8}Fe_2Fe_2Mg_2Fe + \frac{1}{8}Mg_2Fe_2Fe_2Fe + \frac{3}{8}Mg_2Mg_2Mg_2Fe + \frac{3}{28}Fe_2Fe_2Fe_2Fe = \frac{1}{8}Mg_2Fe_2Mg_2Mg + \frac{1}{8}Mg_2Mg_2Fe_2Mg + \frac{1}{8}Fe_2Mg_2Mg_2Mg + \frac{3}{8}Fe_2Fe_2Fe_2Mg + \frac{3}{28}Mg_2Mg_2Mg_2Mg$
	Terms applicable to three-site formulation
$\Delta\overline{G}^0_{ORD,13}$	$\frac{1}{4}Fe_2Fe_2Mg_2Fe + \frac{1}{4}Mg_2Fe_2Fe_2Fe + \frac{1}{4}Mg_2Fe_2Mg_2Fe + \frac{5}{28}Mg_2Mg_2Mg_2Mg = \frac{1}{4}Fe_2Mg_2Fe_2Mg + \frac{1}{4}Mg_2Mg_2Fe_2Mg + \frac{1}{4}Fe_2Mg_2Mg_2Mg + \frac{5}{28}Fe_2Fe_2Fe_2Fe$
	Terms applicable to two-site formulation
$\Delta\overline{G}^0_{ORD,123}$	$\frac{1}{2}Mg_2Fe_2Fe_2Fe + \frac{3}{14}Mg_2Mg_2Mg_2Mg = \frac{1}{2}Fe_2Mg_2Mg_2Mg + \frac{3}{14}Fe_2Fe_2Fe_2Fe$

TABLE 4. Taylor expansion coefficients

$\overline{G}^*_0$	$\frac{\overline{G}^0_{Cm} + \overline{G}^0_{Gn}}{2} + \frac{2W_1 + 2W_2 + W_3 + 2W_4}{4} + \frac{\Delta\overline{G}^0_{X,123,4} + \Delta\overline{G}^0_{X,124,3} + \Delta\overline{G}^0_{X,134,2} + \Delta\overline{G}^0_{X,234,1}}{8}$
$\overline{G}^*_r$	$\frac{\overline{G}^0_{Gn} - \overline{G}^0_{Cm}}{2}$
$\overline{G}^*_{s_1}$	$\Delta\overline{G}^0_{ORD,1}$
$\overline{G}^*_{s_2}$	$\Delta\overline{G}^0_{ORD,2}$
$\overline{G}^*_{s_3}$	$\Delta\overline{G}^0_{ORD,3}$
$\overline{G}^*_{r,r}$	$-\frac{2W_1 + 2W_2 + W_3 + 2W_4}{4} - \frac{\Delta\overline{G}^0_{X,123,4} + \Delta\overline{G}^0_{X,124,3} + \Delta\overline{G}^0_{X,134,2} + \Delta\overline{G}^0_{X,234,1}}{8}$
$\overline{G}^*_{r,s_1}$	$\frac{10W_1 - 4W_2 - 2W_3 - 4W_4}{7} + \frac{5\Delta\overline{G}^0_{X,234,1} - 2\Delta\overline{G}^0_{X,123,4} - 2\Delta\overline{G}^0_{X,124,3} - 2\Delta\overline{G}^0_{X,134,2}}{14}$
$\overline{G}^*_{r,s_2}$	$\frac{10W_2 - 4W_1 - 2W_3 - 4W_4}{7} + \frac{5\Delta\overline{G}^0_{X,134,2} - 2\Delta\overline{G}^0_{X,123,4} - 2\Delta\overline{G}^0_{X,124,3} - 2\Delta\overline{G}^0_{X,234,1}}{14}$
$\overline{G}^*_{r,s_3}$	$\frac{6W_3 - 2W_1 - 2W_2 - 2W_4}{7} + \frac{6\Delta\overline{G}^0_{X,124,3} - \Delta\overline{G}^0_{X,123,4} - \Delta\overline{G}^0_{X,134,2} - \Delta\overline{G}^0_{X,234,1}}{14}$
$\overline{G}^*_{s_1,s_1}$	$-\frac{50W_1 + 8W_2 + 4W_3 + 8W_4}{49} + \frac{12\Delta\overline{G}^0_{X,234,1} - 2\Delta\overline{G}^0_{X,123,4} - 2\Delta\overline{G}^0_{X,124,3} - 2\Delta\overline{G}^0_{X,134,2}}{49}$
$\overline{G}^*_{s_1,s_2}$	$\frac{40W_1 + 40W_2 - 8W_3 - 16W_4}{49} + \frac{\Delta\overline{G}^0_{X,34,12}}{2} - \frac{8\Delta\overline{G}^0_{X,123,4} + 8\Delta\overline{G}^0_{X,124,3} + 29\Delta\overline{G}^0_{X,134,2} + 29\Delta\overline{G}^0_{X,234,1}}{98}$
$\overline{G}^*_{s_1,s_3}$	$\frac{20W_1 + 24W_3 - 8W_2 - 8W_4}{49} + \frac{\Delta\overline{G}^0_{X,13,24}}{2} - \frac{4\Delta\overline{G}^0_{X,123,4} + 25\Delta\overline{G}^0_{X,124,3} + 4\Delta\overline{G}^0_{X,134,2} + 39\Delta\overline{G}^0_{X,234,1}}{98}$
$\overline{G}^*_{s_2,s_2}$	$-\frac{8W_1 + 50W_2 + 4W_3 + 8W_4}{49} + \frac{12\Delta\overline{G}^0_{X,134,2} - 2\Delta\overline{G}^0_{X,123,4} - 2\Delta\overline{G}^0_{X,124,3} - 2\Delta\overline{G}^0_{X,234,1}}{49}$
$\overline{G}^*_{s_2,s_3}$	$\frac{20W_2 + 24W_3 - 8W_1 - 8W_4}{49} - \frac{\Delta\overline{G}^0_{X,13,24} + \Delta\overline{G}^0_{X,34,12}}{2} + \frac{45\Delta\overline{G}^0_{X,123,4} + 24\Delta\overline{G}^0_{X,124,3} + 10\Delta\overline{G}^0_{X,134,2} + 45\Delta\overline{G}^0_{X,234,1}}{98}$
$\overline{G}^*_{s_3,s_3}$	$-\frac{2W_1 + 2W_2 + 36W_3 + 2W_4}{49} + \frac{13\Delta\overline{G}^0_{X,124,3} - \Delta\overline{G}^0_{X,123,4} - \Delta\overline{G}^0_{X,134,2} - \Delta\overline{G}^0_{X,234,1}}{98}$

$$
\begin{aligned}
\overline{G}^* = {} & (\tfrac{2}{7}X^{M1}_{Mg} + \tfrac{2}{7}X^{M2}_{Mg} + \tfrac{1}{7}X^{M3}_{Mg} + \tfrac{2}{7}X^{M4}_{Mg})\overline{G}^0_{Cm} \\
& + (\tfrac{2}{7}X^{M1}_{Fe} + \tfrac{2}{7}X^{M2}_{Fe} + \tfrac{1}{7}X^{M3}_{Fe} + \tfrac{2}{7}X^{M4}_{Fe})\overline{G}^0_{Gn} \\
& + (X^{M4}_{Fe} - X^{M1}_{Fe})\Delta\overline{G}^0_{ORD,1} + (X^{M4}_{Fe} - X^{M2}_{Fe})\Delta\overline{G}^0_{ORD,2} \\
& + (X^{M4}_{Fe} - X^{M3}_{Fe})\Delta\overline{G}^0_{ORD,3} \\
& + (2W_1 + \tfrac{1}{2}\Delta\overline{G}^0_{X,234,1})X^{M1}_{Fe}X^{M1}_{Mg} \\
& + (2W_2 + \tfrac{1}{2}\Delta\overline{G}^0_{X,134,2})X^{M2}_{Fe}X^{M2}_{Mg} \\
& + (W_3 + \tfrac{1}{2}\Delta\overline{G}^0_{X,124,3})X^{M3}_{Fe}X^{M3}_{Mg} \\
& + (2W_4 + \tfrac{1}{2}\Delta\overline{G}^0_{X,123,4})X^{M4}_{Fe}X^{M4}_{Mg} \\
& + \tfrac{1}{2}(X^{M4}_{Fe} - X^{M3}_{Fe})(X^{M2}_{Fe} - X^{M1}_{Fe})\Delta\overline{G}^0_{X,13,24} \\
& + \tfrac{1}{2}(X^{M4}_{Fe} - X^{M2}_{Fe})(X^{M3}_{Fe} - X^{M1}_{Fe})\Delta\overline{G}^0_{X,12,34} \\
& + \tfrac{1}{2}(X^{M1}_{Fe} - X^{M2}_{Fe})(X^{M1}_{Fe} - X^{M3}_{Fe})\Delta\overline{G}^0_{X,234,1} \\
& + \tfrac{1}{2}(X^{M2}_{Fe} - X^{M1}_{Fe})(X^{M2}_{Fe} - X^{M4}_{Fe})\Delta\overline{G}^0_{X,134,2} \\
& + \tfrac{1}{2}(X^{M3}_{Fe} - X^{M1}_{Fe})(X^{M3}_{Fe} - X^{M4}_{Fe})\Delta\overline{G}^0_{X,124,3} \\
& + \tfrac{1}{2}(X^{M4}_{Fe} - X^{M2}_{Fe})(X^{M4}_{Fe} - X^{M3}_{Fe})\Delta\overline{G}^0_{X,123,4}. \qquad (11)
\end{aligned}
$$

The first two terms in Equation 11 represent macroscopic mechanical mixing contributions to $\overline{G}$; the two quantities in parentheses are the bulk mole fractions of Mg and Fe, respectively (Table 1). The next three terms quantify the energetic drive for cation ordering. Values of the parameters $\Delta\overline{G}^0_{ORD,1}$, $\Delta\overline{G}^0_{ORD,2}$, and $\Delta\overline{G}^0_{ORD,3}$, should be negative so that the Gibbs energy of the system will be lowered by preferential occupation of Fe^{2+} on the M4 site (these parameters premultiply the quantities $X^{M4}_{Fe} - X^{i}_{Fe}$). The more negative the value, the greater the partitioning. The four terms involving the intrasite regular-solution parameters (W_1, W_2, W_3, and W_4) describe the energetic consequences of size-mismatch of unlike cations. The quantities in parentheses multiplying each site mole fraction product should be positive, since size-mismatch effects tend to destabilize the solution (Lawson, 1947). Note that the appropriate Fe^{2+}-Mg reciprocal exchange energy enters into these sums and that the site W is multiplied by the stoichiometric number of sites in the formula unit; the W_i is defined on a per cation basis. The remaining six terms in Equation 11 account for the noncoplanarity of the Gibbs energies of vertices of composition-ordering space. They may be thought of as nonmacroscopic contributions to the Gibbs energy of mechanical mixing. Note that the premultiplying mole-fraction terms may be written equivalently using the mole fractions of Mg on the respective sites.

Equations 3, 4, and 11 may be combined and inserted into Equation 9 to provide expressions for the condition of homogeneous equilibrium. We obtain the following:

$$0 = \tfrac{2}{7}RT\ln\left[\left(\frac{X^{M1}_{Mg}}{X^{M1}_{Fe}}\right)^5\left(\frac{X^{M2}_{Fe}}{X^{M2}_{Mg}}\right)^2\left(\frac{X^{M3}_{Fe}}{X^{M3}_{Mg}}\right)\left(\frac{X^{M4}_{Fe}}{X^{M4}_{Mg}}\right)^2\right] + \Delta\overline{G}^0_{ORD,1}$$
$$+ \tfrac{5}{7}(2W_1 + \tfrac{1}{2}\Delta\overline{G}^0_{X,234,1})(X^{M1}_{Fe} - X^{M1}_{Mg})$$
$$- \tfrac{2}{7}(2W_2 + \tfrac{1}{2}\Delta\overline{G}^0_{X,134,2})(X^{M2}_{Fe} - X^{M2}_{Mg})$$
$$- \tfrac{2}{7}(W_3 + \tfrac{1}{2}\Delta\overline{G}^0_{X,124,3})(X^{M3}_{Fe} - X^{M3}_{Mg})$$
$$- \tfrac{2}{7}(2W_4 + \tfrac{1}{2}\Delta\overline{G}^0_{X,123,4})(X^{M4}_{Fe} - X^{M4}_{Mg})$$
$$+ \tfrac{1}{2}(X^{M3}_{Fe} - X^{M1}_{Fe} + X^{M2}_{Fe} - X^{M1}_{Fe})\Delta\overline{G}^0_{X,234,1}$$
$$+ \tfrac{1}{2}(X^{M4}_{Fe} - X^{M3}_{Fe})(\Delta\overline{G}^0_{X,13,24} - \Delta\overline{G}^0_{X,124,3})$$
$$+ \tfrac{1}{2}(X^{M4}_{Fe} - X^{M2}_{Fe})(\Delta\overline{G}^0_{X,12,34} - \Delta\overline{G}^0_{X,134,2}) \qquad (12a)$$

$$0 = \tfrac{2}{7}RT\ln\left[\left(\frac{X^{M1}_{Fe}}{X^{M1}_{Mg}}\right)^2\left(\frac{X^{M2}_{Mg}}{X^{M2}_{Fe}}\right)^5\left(\frac{X^{M3}_{Fe}}{X^{M3}_{Mg}}\right)\left(\frac{X^{M4}_{Fe}}{X^{M4}_{Mg}}\right)^2\right] + \Delta\overline{G}^0_{ORD,2}$$
$$- \tfrac{2}{7}(2W_1 + \tfrac{1}{2}\Delta\overline{G}^0_{X,234,1})(X^{M1}_{Fe} - X^{M1}_{Mg})$$
$$+ \tfrac{5}{7}(2W_2 + \tfrac{1}{2}\Delta\overline{G}^0_{X,134,2})(X^{M2}_{Fe} - X^{M2}_{Mg})$$
$$- \tfrac{2}{7}(W_3 + \tfrac{1}{2}\Delta\overline{G}^0_{X,124,3})(X^{M3}_{Fe} - X^{M3}_{Mg})$$
$$- \tfrac{2}{7}(2W_4 + \tfrac{1}{2}\Delta\overline{G}^0_{X,123,4})(X^{M4}_{Fe} - X^{M4}_{Mg})$$
$$- \tfrac{1}{2}(X^{M4}_{Fe} - X^{M3}_{Fe})(\Delta\overline{G}^0_{X,13,24} - \Delta\overline{G}^0_{X,123,4})$$
$$+ \tfrac{1}{2}(X^{M3}_{Fe} - X^{M1}_{Fe})(\Delta\overline{G}^0_{X,12,34} - \Delta\overline{G}^0_{X,234,1})$$
$$+ \tfrac{1}{2}(X^{M4}_{Fe} - X^{M2}_{Fe} + X^{M1}_{Fe} - X^{M2}_{Fe})\Delta\overline{G}^0_{X,134,2} \qquad (12b)$$

$$0 = \tfrac{2}{7}RT\ln\left[\left(\frac{X^{M1}_{Fe}}{X^{M1}_{Mg}}\right)\left(\frac{X^{M2}_{Fe}}{X^{M2}_{Mg}}\right)\left(\frac{X^{M3}_{Mg}}{X^{M3}_{Fe}}\right)^3\left(\frac{X^{M4}_{Fe}}{X^{M4}_{Mg}}\right)\right] + \Delta\overline{G}^0_{ORD,3}$$
$$- \tfrac{1}{7}(2W_1 + \tfrac{1}{2}\Delta\overline{G}^0_{X,234,1})(X^{M1}_{Fe} - X^{M1}_{Mg})$$
$$- \tfrac{1}{7}(2W_2 + \tfrac{1}{2}\Delta\overline{G}^0_{X,134,2})(X^{M2}_{Fe} - X^{M2}_{Mg})$$
$$+ \tfrac{6}{7}(W_3 + \tfrac{1}{2}\Delta\overline{G}^0_{X,124,3})(X^{M3}_{Fe} - X^{M3}_{Mg})$$
$$- \tfrac{1}{7}(2W_4 + \tfrac{1}{2}\Delta\overline{G}^0_{X,123,4})(X^{M4}_{Fe} - X^{M4}_{Mg})$$
$$+ \tfrac{1}{2}(X^{M2}_{Fe} - X^{M1}_{Fe})(\Delta\overline{G}^0_{X,13,24} - \Delta\overline{G}^0_{X,234,1})$$
$$- \tfrac{1}{2}(X^{M4}_{Fe} - X^{M2}_{Fe})(\Delta\overline{G}^0_{X,12,34} - \Delta\overline{G}^0_{X,123,4})$$
$$+ \tfrac{1}{2}(X^{M4}_{Fe} - X^{M3}_{Fe} + X^{M1}_{Fe} - X^{M3}_{Fe})\Delta\overline{G}^0_{X,124,3}. \qquad (12c)$$

Equations 12a–12c are sufficient to define uniquely the equilibrium ordering state for a given composition, temperature, and pressure (i.e., s_1, s_2, and s_3 as functions of r, T, and P).

The chemical potentials of end-member cummingtonite and grunerite are given according to the extended form of Darken's relation (Ghiorso, 1990b):

$$\mu_{Cm} = \overline{G} - (1+r)\frac{\partial\overline{G}}{\partial r} - s_1\frac{\partial\overline{G}}{\partial s_1} - s_2\frac{\partial\overline{G}}{\partial s_2} - s_3\frac{\partial\overline{G}}{\partial s_3} \qquad (13a)$$

and

$$\mu_{Gn} = \overline{G} + (1-r)\frac{\partial\overline{G}}{\partial r} - s_1\frac{\partial\overline{G}}{\partial s_1} - s_2\frac{\partial\overline{G}}{\partial s_2} - s_2\frac{\partial\overline{G}}{\partial s_3}. \qquad (13b)$$

The Fe^{2+}-Mg exchange potential, $\mu_{Gn} - \mu_{Cm}$, or equivalently $\partial\overline{G}/\partial r$, is given by

$$\frac{\partial\overline{G}}{\partial r} = \tfrac{1}{2}(\overline{G}^0_{Gn} - \overline{G}^0_{Cm})$$
$$+ \tfrac{1}{2}RT\ln\left[\left(\frac{X^{M1}_{Fe}}{X^{M1}_{Mg}}\right)^2\left(\frac{X^{M2}_{Fe}}{X^{M2}_{Mg}}\right)^2\left(\frac{X^{M3}_{Fe}}{X^{M3}_{Mg}}\right)\left(\frac{X^{M4}_{Fe}}{X^{M4}_{Mg}}\right)^2\right]$$
$$- \tfrac{1}{2}(2W_1 + \tfrac{1}{2}\Delta\overline{G}^0_{X,234,1})(X^{M1}_{Fe} - X^{M1}_{Mg})$$
$$- \tfrac{1}{2}(2W_2 + \tfrac{1}{2}\Delta\overline{G}^0_{X,134,2})(X^{M2}_{Fe} - X^{M2}_{Mg})$$
$$- \tfrac{1}{2}(W_3 + \tfrac{1}{2}\Delta\overline{G}^0_{X,124,3})(X^{M3}_{Fe} - X^{M3}_{Mg})$$
$$- \tfrac{1}{2}(2W_4 + \tfrac{1}{2}\Delta\overline{G}^0_{X,123,4})(X^{M4}_{Fe} - X^{M4}_{Mg}). \qquad (14)$$

Substitution of Equations 3, 4, 11, 12, and 14 into Equation 13 provides model expressions for the end-member potentials:

$$\mu_{Cm} = \overline{G}^0_{Cm} + RT(2\ln X^{M1}_{Mg} + 2\ln X^{M2}_{Mg} + \ln X^{M3}_{Mg} + 2\ln X^{M4}_{Mg})$$
$$+ (2W_1 + \tfrac{1}{2}\Delta\overline{G}^0_{X,234,1})X^{M1}_{Fe}X^{M1}_{Fe}$$
$$+ (2W_2 + \tfrac{1}{2}\Delta\overline{G}^0_{X,134,2})X^{M2}_{Fe}X^{M2}_{Fe}$$
$$+ (W_3 + \tfrac{1}{2}\Delta\overline{G}^0_{X,124,3})X^{M3}_{Fe}X^{M3}_{Fe}$$
$$+ (2W_4 + \tfrac{1}{2}\Delta\overline{G}^0_{X,123,4})X^{M4}_{Fe}X^{M4}_{Fe}$$
$$- \tfrac{1}{2}(X^{M4}_{Fe} - X^{M3}_{Fe})(X^{M2}_{Fe} - X^{M1}_{Fe})\Delta\overline{G}^0_{X,13,24}$$
$$- \tfrac{1}{2}(X^{M4}_{Fe} - X^{M2}_{Fe})(X^{M3}_{Fe} - X^{M1}_{Fe})\Delta\overline{G}^0_{X,12,34}$$
$$- \tfrac{1}{2}(X^{M1}_{Fe} - X^{M2}_{Fe})(X^{M1}_{Fe} - X^{M3}_{Fe})\Delta\overline{G}^0_{X,234,1}$$
$$- \tfrac{1}{2}(X^{M2}_{Fe} - X^{M1}_{Fe})(X^{M2}_{Fe} - X^{M4}_{Fe})\Delta\overline{G}^0_{X,134,2}$$
$$- \tfrac{1}{2}(X^{M3}_{Fe} - X^{M1}_{Fe})(X^{M3}_{Fe} - X^{M4}_{Fe})\Delta\overline{G}^0_{X,124,3}$$
$$- \tfrac{1}{2}(X^{M4}_{Fe} - X^{M2}_{Fe})(X^{M4}_{Fe} - X^{M3}_{Fe})\Delta\overline{G}^0_{X,123,4} \qquad (15a)$$

$$\mu_{Gn} = \overline{G}^0_{Gn} + RT(2\ln X^{M1}_{Fe} + 2\ln X^{M2}_{Fe} + \ln X^{M3}_{Fe} + 2\ln X^{M4}_{Fe})$$
$$+ (2W_1 + \tfrac{1}{2}\Delta\overline{G}^0_{X,234,1})X^{M1}_{Mg}X^{M1}_{Mg}$$
$$+ (2W_2 + \tfrac{1}{2}\Delta\overline{G}^0_{X,134,2})X^{M2}_{Mg}X^{M2}_{Mg}$$
$$+ (W_3 + \tfrac{1}{2}\Delta\overline{G}^0_{X,124,3})X^{M3}_{Mg}X^{M3}_{Mg}$$
$$+ (2W_4 + \tfrac{1}{2}\Delta\overline{G}^0_{X,123,4})X^{M4}_{Mg}X^{M4}_{Mg}$$
$$- \tfrac{1}{2}(X^{M4}_{Fe} - X^{M3}_{Fe})(X^{M2}_{Fe} - X^{M1}_{Fe})\Delta\overline{G}^0_{X,13,24}$$
$$- \tfrac{1}{2}(X^{M4}_{Fe} - X^{M2}_{Fe})(X^{M3}_{Fe} - X^{M1}_{Fe})\Delta\overline{G}^0_{X,12,34}$$
$$- \tfrac{1}{2}(X^{M1}_{Fe} - X^{M2}_{Fe})(X^{M1}_{Fe} - X^{M3}_{Fe})\Delta\overline{G}^0_{X,234,1}$$
$$- \tfrac{1}{2}(X^{M2}_{Fe} - X^{M1}_{Fe})(X^{M2}_{Fe} - X^{M4}_{Fe})\Delta\overline{G}^0_{X,134,2}$$
$$- \tfrac{1}{2}(X^{M3}_{Fe} - X^{M1}_{Fe})(X^{M3}_{Fe} - X^{M4}_{Fe})\Delta\overline{G}^0_{X,124,3}$$
$$- \tfrac{1}{2}(X^{M4}_{Fe} - X^{M2}_{Fe})(X^{M4}_{Fe} - X^{M3}_{Fe})\Delta\overline{G}^0_{X,123,4}. \qquad (15b)$$

TABLE 5. Three-site approximation and model equations

Expression	Ref. no.
$\overline{G} = (\tfrac{3}{7}X_{Mg}^{M13} + \tfrac{2}{7}X_{Mg}^{M2} + \tfrac{2}{7}X_{Mg}^{M4})\overline{G}^{0}_{Cm} + (\tfrac{3}{7}X_{Fe}^{M13} + \tfrac{2}{7}X_{Fe}^{M2} + \tfrac{2}{7}X_{Fe}^{M4})\overline{G}^{0}_{Gn}$ $+ RT(3X_{Fe}^{M13}\ln X_{Fe}^{M13} + 3X_{Mg}^{M13}\ln X_{Mg}^{M13} + 2X_{Fe}^{M2}\ln X_{Fe}^{M2} + 2X_{Mg}^{M2}\ln X_{Mg}^{M2} + 2X_{Fe}^{M4}\ln X_{Fe}^{M4} + 2X_{Mg}^{M4}\ln X_{Mg}^{M4})$ $+ (X_{Fe}^{M4} - X_{Fe}^{M13})(\Delta\overline{G}^{0}_{ORD,1} + \Delta\overline{G}^{0}_{ORD,3}) + (X_{Fe}^{M4} - X_{Fe}^{M2})\Delta\overline{G}^{0}_{ORD,2} + (3W_{13} + \tfrac{1}{2}\Delta\overline{G}^{0}_{X,13,24})X_{Fe}^{M13}X_{Mg}^{M13} + (2W_2 + \tfrac{1}{2}\Delta\overline{G}^{0}_{X,134,2})X_{Fe}^{M2}X_{Mg}^{M2}$ $+ (2W_4 + \tfrac{1}{2}\Delta\overline{G}^{0}_{X,123,4})X_{Fe}^{M4}X_{Mg}^{M4} + \tfrac{1}{2}(X_{Fe}^{M4} - X_{Fe}^{M13})(X_{Fe}^{M2} - X_{Fe}^{M13})\Delta\overline{G}^{0}_{X,13,24} + \tfrac{1}{2}(X_{Fe}^{M2} - X_{Fe}^{M13})(X_{Fe}^{M2} - X_{Fe}^{M4})\Delta\overline{G}^{0}_{X,134,2}$ $+ \tfrac{1}{2}(X_{Fe}^{M4} - X_{Fe}^{M2})(X_{Fe}^{M4} - X_{Fe}^{M13})\Delta\overline{G}^{0}_{X,123,4}$	T5-1
$\dfrac{\partial\overline{G}}{\partial r} = \tfrac{1}{2}(\overline{G}^{0}_{Gn} - \overline{G}^{0}_{Cm}) + \tfrac{1}{2}RT\ln\left[\left(\dfrac{X_{Fe}^{M13}}{X_{Mg}^{M13}}\right)^{3}\left(\dfrac{X_{Fe}^{M2}}{X_{Mg}^{M2}}\right)^{2}\left(\dfrac{X_{Fe}^{M4}}{X_{Mg}^{M4}}\right)^{2}\right] - \tfrac{1}{2}(3W_{13} + \tfrac{1}{2}\Delta\overline{G}^{0}_{X,13,24})(X_{Fe}^{M13} - X_{Mg}^{M13}) - \tfrac{1}{2}(2W_2 + \tfrac{1}{2}\Delta\overline{G}^{0}_{X,134,2})(X_{Fe}^{M2} - X_{Mg}^{M2})$ $- \tfrac{1}{2}(2W_4 + \tfrac{1}{2}\Delta\overline{G}^{0}_{X,123,4})(X_{Fe}^{M4} - X_{Mg}^{M4})$	T5-2
$\dfrac{\partial\overline{G}}{\partial s_{13}} = \Delta\overline{G}^{0}_{ORD,1} + \Delta\overline{G}^{0}_{ORD,3} + \tfrac{6}{7}RT\ln\left[\left(\dfrac{X_{Mg}^{M13}}{X_{Fe}^{M13}}\right)^{2}\left(\dfrac{X_{Fe}^{M2}}{X_{Mg}^{M2}}\right)\left(\dfrac{X_{Fe}^{M4}}{X_{Mg}^{M4}}\right)\right] + \tfrac{4}{7}(3W_{13} + \tfrac{1}{2}\Delta\overline{G}^{0}_{X,13,24})(X_{Fe}^{M13} - X_{Mg}^{M13}) - \tfrac{3}{7}(2W_2 + \tfrac{1}{2}\Delta\overline{G}^{0}_{X,134,2})(X_{Fe}^{M2} - X_{Mg}^{M2})$ $- \tfrac{3}{7}(2W_4 + \tfrac{1}{2}\Delta\overline{G}^{0}_{X,123,4})(X_{Fe}^{M4} - X_{Mg}^{M4}) + \tfrac{1}{2}(X_{Fe}^{M4} - X_{Fe}^{M13})\Delta\overline{G}^{0}_{X,13,24} + \tfrac{1}{2}(X_{Fe}^{M4} - X_{Fe}^{M2})(\Delta\overline{G}^{0}_{X,123,4} - \Delta\overline{G}^{0}_{X,134,2})$	T5-3a
$\dfrac{\partial\overline{G}}{\partial s_{2}} = \Delta\overline{G}^{0}_{ORD,2} + \tfrac{2}{7}RT\ln\left[\left(\dfrac{X_{Fe}^{M13}}{X_{Mg}^{M13}}\right)^{3}\left(\dfrac{X_{Mg}^{M2}}{X_{Fe}^{M2}}\right)^{5}\left(\dfrac{X_{Fe}^{M4}}{X_{Mg}^{M4}}\right)^{2}\right] - \tfrac{2}{7}(3W_{13} + \tfrac{1}{2}\Delta\overline{G}^{0}_{X,13,24})(X_{Fe}^{M13} - X_{Mg}^{M13}) + \tfrac{5}{7}(2W_2 + \tfrac{1}{2}\Delta\overline{G}^{0}_{X,134,2})(X_{Fe}^{M2} - X_{Mg}^{M2})$ $- \tfrac{2}{7}(2W_4 + \tfrac{1}{2}\Delta\overline{G}^{0}_{X,123,4})(X_{Fe}^{M4} - X_{Mg}^{M4}) + \tfrac{1}{2}(X_{Fe}^{M4} - X_{Fe}^{M2} + X_{Fe}^{M13} - X_{Fe}^{M2})\Delta\overline{G}^{0}_{X,134,2} - \tfrac{1}{2}(X_{Fe}^{M4} - X_{Fe}^{M13})(\Delta\overline{G}^{0}_{X,13,24} - \Delta\overline{G}^{0}_{X,123,4})$	T5-3b
$\mu_{Cm} = \overline{G}^{0}_{Cm} + RT(3\ln X_{Mg}^{M13} + 2\ln X_{Mg}^{M2} + 2\ln X_{Mg}^{M4}) + (3W_{13} + \tfrac{1}{2}\overline{G}^{0}_{X,13,24})X_{Fe}^{M13}X_{Fe}^{M13} + (2W_2 + \tfrac{1}{2}\Delta\overline{G}^{0}_{X,134,2})X_{Fe}^{M2}X_{Fe}^{M2}$ $+ (2W_4 + \tfrac{1}{2}\Delta\overline{G}^{0}_{X,123,4})X_{Fe}^{M4}X_{Fe}^{M4} - \tfrac{1}{2}(X_{Fe}^{M4} - X_{Fe}^{M13})(X_{Fe}^{M2} - X_{Fe}^{M13})\Delta\overline{G}^{0}_{X,13,24} - \tfrac{1}{2}(X_{Fe}^{M2} - X_{Fe}^{M13})(X_{Fe}^{M2} - X_{Fe}^{M4})\Delta\overline{G}^{0}_{X,134,2}$ $- \tfrac{1}{2}(X_{Fe}^{M4} - X_{Fe}^{M2})(X_{Fe}^{M4} - X_{Fe}^{M13})\Delta\overline{G}^{0}_{X,123,4}$	T5-4a
$\mu_{Gn} = \overline{G}^{0}_{Gn} + RT(3\ln X_{Fe}^{M13} + 2\ln X_{Fe}^{M2} + 2\ln X_{Fe}^{M4}) + (3W_{13} + \tfrac{1}{2}\overline{G}^{0}_{X,13,24})X_{Mg}^{M13}X_{Mg}^{M13} + (2W_2 + \tfrac{1}{2}\Delta\overline{G}^{0}_{X,134,2})X_{Mg}^{M2}X_{Mg}^{M2}$ $+ (2W_4 + \tfrac{1}{2}\Delta\overline{G}^{0}_{X,123,4})X_{Mg}^{M4}X_{Mg}^{M4} - \tfrac{1}{2}(X_{Fe}^{M4} - X_{Fe}^{M13})(X_{Fe}^{M2} - X_{Fe}^{M13})\Delta\overline{G}^{0}_{X,13,24} - \tfrac{1}{2}(X_{Fe}^{M2} - X_{Fe}^{M13})(X_{Fe}^{M2} - X_{Fe}^{M4})\Delta\overline{G}^{0}_{X,134,2}$ $- \tfrac{1}{2}(X_{Fe}^{M4} - X_{Fe}^{M2})(X_{Fe}^{M4} - X_{Fe}^{M13})\Delta\overline{G}^{0}_{X,123,4}$	T5-4b

Reduction to a three- or two-site formulation

The model equations developed above may be simplified in the case where experimental data or required accuracy in application do not warrant the full four-site expansion. Expressions may be readily developed under the assumption of random mixing (absence of Fe^{2+}-Mg ordering) over the M1 and M3 sites (the three-site model) or the assumption of random mixing over the M1, M2, and M3 sites (the two-site model). For the former it is convenient to define the pseudo intrasite regular-solution parameter, W_{13}, corresponding to the $Mg_7Si_8O_{22}(OH)_2$-$Mg_2^{M4}Fe_2^{M1}Mg_2^{M2}Fe^{M3}Si_8O_{22}(OH)_2$ join. By utilizing Equation 11 to evaluate directly the Gibbs energy at the midpoint of this join, it can be demonstrated that W_{13} is related to W_1 and W_3 by the following:

$$3W_{13} + \tfrac{1}{2}\Delta\overline{G}^{0}_{X,13,24} = (2W_1 + \tfrac{1}{2}\Delta\overline{G}^{0}_{X,234,1}) + (W_3 + \tfrac{1}{2}\Delta\overline{G}^{0}_{X,124,3}). \quad (16)$$

Similarly for the two-site model, we define the parameter

TABLE 6. Two-site approximation

Expression	Ref. no.
$\overline{G} = (\tfrac{5}{7}X_{Mg}^{M123} + \tfrac{2}{7}X_{Mg}^{M4})\overline{G}^{0}_{Cm} + (\tfrac{5}{7}X_{Fe}^{M123} + \tfrac{2}{7}X_{Fe}^{M4})\overline{G}^{0}_{Gn} + RT(5X_{Fe}^{M123}\ln X_{Fe}^{M123} + 5X_{Mg}^{M123}\ln X_{Mg}^{M123} + 2X_{Fe}^{M4}\ln X_{Fe}^{M4} + 2X_{Mg}^{M4}\ln X_{Mg}^{M4})$ $+ (X_{Fe}^{M4} - X_{Fe}^{M123})(\Delta\overline{G}^{0}_{ORD,1} + \Delta\overline{G}^{0}_{ORD,2} + \Delta\overline{G}^{0}_{ORD,3}) + (5W_{123} + \tfrac{1}{2}\Delta\overline{G}^{0}_{X,123,4})X_{Fe}^{M123}X_{Mg}^{M123}$ $+ (2W_4 + \tfrac{1}{2}\Delta\overline{G}^{0}_{X,123,4})X_{Fe}^{M4}X_{Mg}^{M4} + \tfrac{1}{2}(X_{Fe}^{M4} - X_{Fe}^{M123})^2\Delta\overline{G}^{0}_{X,123,4}$	T6-1
$\dfrac{\partial\overline{G}}{\partial r} = \tfrac{1}{2}(\overline{G}^{0}_{Gn} - \overline{G}^{0}_{Cm}) + \tfrac{1}{2}RT\ln\left[\left(\dfrac{X_{Fe}^{M123}}{X_{Mg}^{M123}}\right)^{5}\left(\dfrac{X_{Fe}^{M4}}{X_{Mg}^{M4}}\right)^{2}\right] - \tfrac{1}{2}(5W_{123} + \tfrac{1}{2}\Delta\overline{G}^{0}_{X,123,4})(X_{Fe}^{M123} - X_{Mg}^{M123}) - \tfrac{1}{2}(2W_4 + \tfrac{1}{2}\Delta\overline{G}^{0}_{X,123,4})(X_{Fe}^{M4} - X_{Mg}^{M4})$	T6-2
$\dfrac{\partial\overline{G}}{\partial s_{123}} = \Delta\overline{G}^{0}_{ORD,1} + \Delta\overline{G}^{0}_{ORD,2} + \Delta\overline{G}^{0}_{ORD,3} + \tfrac{1}{7}\ln\left[\left(\dfrac{X_{Mg}^{M123}}{X_{Fe}^{M123}}\right)\left(\dfrac{X_{Fe}^{M4}}{X_{Mg}^{M4}}\right)\right] + \tfrac{2}{7}(5W_{123} + \tfrac{1}{2}\Delta\overline{G}^{0}_{X,123,4})(X_{Fe}^{M123} - X_{Mg}^{M123})$ $- \tfrac{5}{7}(2W_4 + \tfrac{1}{2}\Delta\overline{G}^{0}_{X,123,4})(X_{Fe}^{M4} - X_{Mg}^{M4}) + (X_{Fe}^{M4} - X_{Fe}^{M123})\Delta\overline{G}^{0}_{X,123,4}$	T6-3
$\mu_{Cm} = \overline{G}^{0}_{Cm} + RT(5\ln X_{Mg}^{M123} + 2\ln X_{Mg}^{M4}) + (5W_{123} + \tfrac{1}{2}\Delta\overline{G}^{0}_{X,123,4})X_{Fe}^{M123}X_{Fe}^{M123} + (2W_4 + \tfrac{1}{2}\Delta\overline{G}^{0}_{X,123,4})X_{Fe}^{M4}X_{Fe}^{M4} - \tfrac{1}{2}(X_{Fe}^{M4} - X_{Fe}^{M123})^2\Delta\overline{G}^{0}_{X,123,4}$	T6-4a
$\mu_{Gn} = \overline{G}^{0}_{Gn} + RT(5\ln X_{Fe}^{M123} + 2\ln X_{Fe}^{M4}) + (5W_{123} + \tfrac{1}{2}\Delta\overline{G}^{0}_{X,123,4})X_{Mg}^{M123}X_{Mg}^{M123} + (2W_4 + \tfrac{1}{2}\Delta\overline{G}^{0}_{X,123,4})X_{Mg}^{M4}X_{Mg}^{M4} - \tfrac{1}{2}(X_{Fe}^{M4} - X_{Fe}^{M123})^2\Delta\overline{G}^{0}_{X,123,4}$	T6-4b

W_{123}, corresponding to the join $Mg_7Si_8O_{22}(OH)_2$-$Mg_2^{M4}Fe_2^{M1}Fe_2^{M2}Fe^{M3}Si_8O_{22}(OH)_2$. Evaluating Equation 11 provides the identity

$$5W_{123} + \tfrac{1}{2}\Delta\overline{G}^0_{X,123,4} = (2W_1 + \tfrac{1}{2}\Delta\overline{G}^0_{X,234,1}) + (2W_2 + \tfrac{1}{2}\Delta\overline{G}^0_{X,134,2}) + (W_3 + \tfrac{1}{2}\Delta\overline{G}^0_{X,124,3}). \quad (17)$$

It follows that W_{123} and W_{13} are related:

$$5W_{123} + \tfrac{1}{2}\Delta\overline{G}^0_{X,123,4} = (3W_{13} + \tfrac{1}{2}\Delta\overline{G}^0_{X,13,24}) + (2W_2 + \tfrac{1}{2}\Delta\overline{G}^0_{X,134,2}). \quad (18)$$

A model expression for $\overline{G}$ in the three-site approximation may be obtained from Equations 3, 4, and 11 by substituting Equation 16 and the identities

$$X^{M13}_{Fe} = X^{M1}_{Fe} = X^{M3}_{Fe} \quad (19a)$$

and

$$X^{M13}_{Mg} = X^{M1}_{Mg} = X^{M3}_{Mg}. \quad (19b)$$

The resulting expression for $\overline{G}$ is provided in Table 5 (Eq. T5-1). The remaining entries in the table are obtained in a similar manner. Notice that in the three-site approximation, s_1 is equal to s_3,

$$\frac{\partial\overline{G}}{\partial s_{13}} = \frac{\partial\overline{G}}{\partial s_1} + \frac{\partial\overline{G}}{\partial s_3} \quad (20)$$

and consequently

$$\Delta\overline{G}^0_{ORD,13} = \Delta\overline{G}^0_{ORD,1} + \Delta\overline{G}^0_{ORD,3}. \quad (21)$$

Thus, the number of (preferred) parameters has been reduced from 15 to 10. Model expressions in the two-site approximation are provided in Table 6 and result from Equation 17 and the identities

$$X^{M123}_{Fe} = X^{M1}_{Fe} = X^{M2}_{Fe} = X^{M3}_{Fe} \quad (22a)$$

$$X^{M123}_{Mg} = X^{M1}_{Mg} = X^{M2}_{Mg} = X^{M3}_{Mg} \quad (22b)$$

$$\frac{\partial\overline{G}}{\partial s_{123}} = \frac{\partial\overline{G}}{\partial s_1} + \frac{\partial\overline{G}}{\partial s_2} + \frac{\partial\overline{G}}{\partial s_3} \quad (23)$$

and

$$\Delta\overline{G}^0_{ORD,123} = \Delta\overline{G}^0_{ORD,1} + \Delta\overline{G}^0_{ORD,2} + \Delta\overline{G}^0_{ORD,3}. \quad (24)$$

This further reduces the number of (preferred) parameters to six.

Calibration

Calibration of our model requires three sorts of data: (1) constraints on the standard-state properties, including heat capacities and volumes as a function of T and P, as well as reference-state entropies and enthalpies, (2) constraints on Fe^{2+}-Mg^{2+} cation ordering as a function of temperature, pressure, and bulk composition, and (3) constraints on the conditions of heterogeneous equilibrium between coexisting ferromagnesian amphibole and other thermodynamically well-characterized phases (e.g., orthopyroxene, olivine, and spinel). The first of these datasets allows estimation of the temperature and pressure dependence of the end-member quantities $\overline{G}^0_{Cm}$ and $\overline{G}^0_{Gn}$. The second and third datasets constrain the remaining solution parameters. We discuss the available data and methods of calibration below.

TABLE 7. Internally consistent thermodynamic properties of end-member solids

	Anthophyllite $Mg_7Si_8O_{22}(OH)_2$	Cummingtonite $Mg_7Si_8O_{22}(OH)_2$	Grunerite $Fe_7Si_8O_{22}(OH)_2$
$\Delta\overline{H}^0_f$ (kJ)	−12073.132	−12067.517	−9623.300
$\overline{S}^0$ (J/K)	535.259	540.259	725
$\overline{V}^0$ (J/bar)	26.33		27.84
k_0	1233.8		1347.83
$k_1 \times 10^{-2}$	−71.3398		−93.5691
$k_2 \times 10^{-5}$	−221.638		−202.285
$k_3 \times 10^{-7}$	233.394		303.919
$v_1 \times 10^6$	−1.1394		−1.6703
$v_2 \times 10^{12}$			8.68919
$v_3 \times 10^6$	28.105		28.400
$v_4 \times 10^{10}$	62.894		

Note: $\overline{C}^0_P = k_0 + (k_1/\sqrt{T}) + (k_2/T^2) + (k_3/T^3)$ (J/K). $\overline{V}/\overline{V}^0 = 1 + v_1(P - P_r) + v_2(P - P_r)^2 + v_3(T - T_r) + v_4(T - T_r)^2$ (J/bar). $\Delta\overline{H}^0_f$ and $\overline{S}^0$ of anthophyllite and cummingtonite are given with greater precision than individually known in order to maintain internal consistency.

Standard-state data

Standard-state properties of grunerite (Table 7) are referenced to those of fayalite, ferrosilite, quartz, and H_2O after Berman (1988). Molar volume is taken from the extrapolation by Hirschmann et al. (1994) of natural cummingtonite cell volumes corrected for Ca and Mn. Expansivity is from Holland and Powell (1990). Compressibility was fit as a binomial to the data of Zhang et al. (1992). Enthalpy of formation was adjusted so as to fit the half-brackets at high P and T on the breakdown reactions of grunerite

$$\underset{\text{grunerite}}{Fe_7Si_8O_{22}(OH)_2} = \underset{\text{ferrosilite}}{7FeSiO_3} + \underset{\text{quartz}}{SiO_2} + \underset{\text{water}}{H_2O} \quad (25)$$

and

$$\underset{\text{grunerite}}{Fe_7Si_8O_{22}(OH)_2} = \underset{\text{fayalite}}{\tfrac{7}{2}Fe_2SiO_4} + \underset{\text{quartz}}{\tfrac{9}{2}SiO_2} + \underset{\text{water}}{H_2O} \quad (26)$$

by Lattard and Evans (1992). At the same time, the entropy of grunerite was adjusted downwards to 725 J/K from 734 ± 7 J/K (Holland, 1989) and 730 J/K (calculated by Lattard and Evans, 1992, after Anovitz et al., 1988) in order to optimize the fit to the experimental data.

Standard-state properties of magnesio-cummingtonite (Table 7) are based with minor modification on those of anthophyllite (R. G. Berman, 1990 personal communication), which are consistent with other MgO-SiO_2-H_2O minerals in the Berman (1988) database. Compositional data from the literature on natural olivine-anthophyllite and olivine-cummingtonite pairs are consistent with independent literature data on anthophyllite-cummingtonite pairs (extrapolated Al-free) in indicating, in the compositional range of metamorphic ultramafic rocks (X_{Fa} in

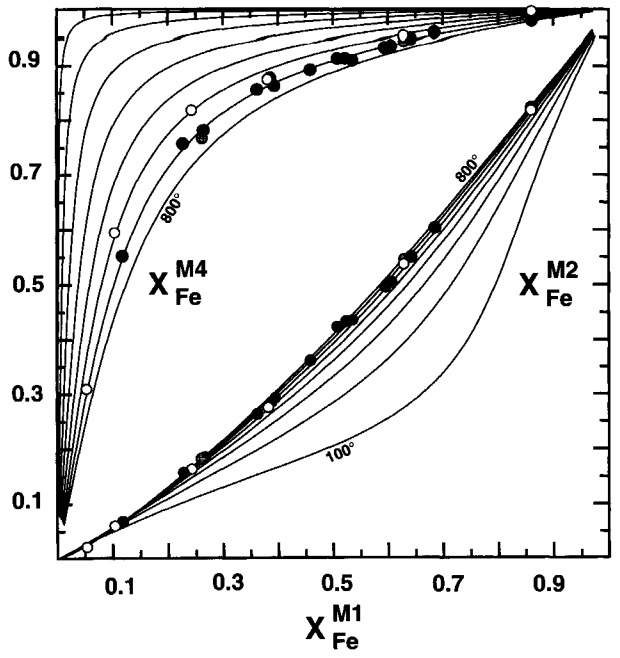

Fig. 1. Roozeboom plots of X_{Fe}^{M4} and X_{Fe}^{M2} vs. X_{Fe}^{M1} in cummingtonite. Projected from X-ray refinements of reequilibrated natural cummingtonite (Hirschmann et al., 1994): 750 °C, gray circles; 700 °C, black circles; 600 °C, open circles. Isotherms computed in this study ($X_{Fe}^{M1} = X_{Fe}^{M3}$).

olivine 5–20%), a value for $\Delta\overline{G}^0$ for the exchange equilibrium

$$\underset{\text{magnesio-anthophyllite}}{Mg_7Si_8O_{22}(OH)_2} + \underset{\text{grunerite}}{Fe_7Si_8O_{22}(OH)_2} = \underset{\text{ferro-anthophyllite}}{Fe_7Si_8O_{22}(OH)_2} + \underset{\text{magnesio-cummingtonite}}{Mg_7Si_8O_{22}(OH)_2} \quad (27)$$

to be 1.1kJ/cation at 650 °C with an estimated uncertainty (2σ) of 0.5 kJ/cation. Since Mg-Fe^{2+} cation order at high temperature in Mg-rich anthophyllite and cummingtonite is apparently indistinguishable (Hirschmann et al., 1994), we assume cancellation of nonideal properties in the equilibrium

$$\underset{\text{magnesio-anthophyllite}}{Mg_7Si_8O_{22}(OH)_2} = \underset{\text{magnesio-cummingtonite}}{Mg_7Si_8O_{22}(OH)_2} \quad (28)$$

and derive from the Mg-Fe partitioning data a (rounded-off) $\Delta\overline{G}^0$ for the dimorphic transition at 650 °C of 1.0 kJ/mol.

The entropy of magnesio-cummingtonite has not been determined by calorimetry. We concur with the belief that cummingtonite is the high-temperature form (Ross et al., 1969; Prewitt et al., 1970; Ghose, 1981; Carpenter, 1982) and accordingly adopt a provisional $\overline{S}^0$ (1 bar, 298 K) of magnesio-cummingtonite that is 5 J/K larger than $\overline{S}^0$ anthophyllite, an amount that is consistent with their virtually indistinguishable molar volumes (Hirschmann et al., 1994) and with data for analogous pyroxenes. A reaction entropy any larger than 5 J/K would stabilize magnesio-cummingtonite below 850 °C, and, so far, syntheses of magnesium amphibole in the system MgO-SiO_2-H_2O (up to 815 °C) have always been reported as orthorhombic (Greenwood, 1963; Chernosky et al., 1985). The 298 K entropy of anthophyllite (incorporating phase-equilibrium constraints) is 535.3 J/K (Table 7), which is slightly larger than the calorimetric value of 534.5 J/K but well within its ±3.5 J/K uncertainty (Hemingway, 1991).

The high-temperature heat capacity, expansivity, and compressibility of magnesio-anthophyllite and magnesio-cummingtonite are assumed to be identical. Given the above estimates of reaction entropy at 298 K and reaction free energy at 650 °C, we therefore arrive at a temperature-independent enthalpy for Reaction 28 of 5615 J/mol.

Cation ordering constraints

In Figure 1 we plot data from Hirschmann et al. (1994) on the distribution of Fe^{2+} between M4 and M1, and M1 and M2 sites in ferromagnesian clinoamphiboles. The data were obtained by single-crystal X-ray structure refinements of naturally occurring cummingtonite heat-treated and quenched from the indicated temperatures. These data are consistent with, but supersede in quality and precision, the data of previous studies of cummingtonite cation ordering (e.g., Bancroft et al., 1967; Hafner and Ghose, 1971; Ghose and Weidner, 1972; Barabanov and Tomilov, 1973) obtained for the most part using Mössbauer methods, which do not distinguish the M1, M2, and M3 sites. Fe^{2+} is strongly partitioned between M4 and M1(M3) and between M4 and M2. It is weakly partitioned between M2 and M1(M3). Fe^{2+} and Mg are randomly distributed (within experimental uncertainty) between M1 and M3 (Hirschmann et al., 1994). The data plotted in Figure 1 provide a basis for calibrating model parameters appropriate for the three-site formulation (Table 5).

In order to proceed, we must first recognize that data on cation ordering, no matter how precise, cannot constrain uniquely all eight mixing parameters of the three-site model (i.e., all of W_2, W_{13}, W_4, $\Delta\bar{G}^0_{X,123,4}$, $\Delta\overline{G}^0_{X,134,2}$, $\Delta\overline{G}^0_{X,13,24}$, $\delta\overline{G}^0_{ORD,2}$, and $\Delta\overline{G}^0_{ORD,13}$). The easiest way to see this is to differentiate an expression for the molar Gibbs free energy of solution in the three-site approximation (reducing Eqs. 3, 4, and 5 from the four-site to the three-site formulation),

$$\begin{aligned}\overline{G} = &-T\overline{S}_{conf} + \overline{G}^*_0 + \overline{G}^*_r r + \overline{G}^*_{s_{13}} s_{13} + \overline{G}^*_{s_2} s_2 + \overline{G}^*_{r,r} r^2 \\ &+ \overline{G}^*_{r,s_{13}} r s_{13} + \overline{G}^*_{r,s_2} r s_2 + \overline{G}^*_{s_{13},s_{13}} s^2_{13} + \overline{G}^*_{s_{13},s_2} s_{13} s_2 \\ &+ \overline{G}^*_{s_2,s_2} s^2_2 \end{aligned} \quad (29)$$

with respect to s_{13} and s_2, in order to obtain conditions for homogeneous equilibrium as a function of the Taylor expansion coefficients of $\overline{G}^*$:

TABLE 8. Values and correlation of Taylor expansion coefficients from cation-ordering fits

	$\overline{G}^*_{s_{13}}$	$\overline{G}^*_{s_2}$	$\overline{G}^*_{r,s_{13}}$	$\overline{G}^*_{r,s_2}$	$\overline{G}^*_{s_{13},s_{13}}$	$\overline{G}^*_{s_{13},s_2}$	$\overline{G}^*_{s_2,s_2}$
Value (kJ)	−9.608	−16.248	−3.776	3.405	−8.784	8.579	−3.046
Std. err.	0.803	0.998	0.985	0.943	5.067	7.977	3.008
$\overline{G}^*_{s_{13}}$	1						
$\overline{G}^*_{s_2}$	−0.605	1					
$\overline{G}^*_{r,s_{13}}$	−0.661	0.798	1				
$\overline{G}^*_{r,s_2}$	0.671	−0.859	−0.907	1			
$\overline{G}^*_{s_{13},s_{13}}$	−0.405	0.538	0.849	−0.799	1		
$\overline{G}^*_{s_{13},s_2}$	0.251	−0.463	−0.780	0.730	−0.987	1	
$\overline{G}^*_{s_2,s_2}$	−0.0986	0.215	0.628	−0.552	0.928	−0.965	1

$$\frac{\partial \overline{G}}{\partial s_{13}} = 0 = -T\frac{\partial \overline{S}_{\text{conf}}}{\partial s_{13}} + \overline{G}^*_{s_{13}} + \overline{G}^*_{r,s_{13}} r + 2\overline{G}^*_{s_{13},s_{13}} s_{13} + \overline{G}^*_{s_{13},s_2} s_2 \quad (30a)$$

$$\frac{\partial \overline{G}}{\partial s_2} = 0 = -T\frac{\partial \overline{S}_{\text{conf}}}{\partial s_2} + \overline{G}^*_{s_2} + \overline{G}^*_{r,s_2} r + \overline{G}^*_{s_{13},s_2} s_{13} + 2\overline{G}^*_{s_2,s_2} s_2. \quad (30b)$$

These conditions, which define the cation-ordering constraints depicted in Figure 1, involve seven Taylor expansion coefficients and consequently afford the possibility of calibrating only seven of the preferred model parameters. As demonstrated in Table 4, linear combinations of the preferred model parameters may be rearranged to provide definitions for the Taylor expansion coefficients. Inverting this system of equations we obtain the following:

$$\overline{G}^0_{\text{Cm}} = \overline{G}^*_0 - \overline{G}^*_r + \overline{G}^*_{r,r} \quad (31a)$$

$$\overline{G}^0_{\text{Gn}} = \overline{G}^*_0 + \overline{G}^*_r + \overline{G}^*_{r,r} \quad (31b)$$

$$\Delta\overline{G}^0_{\text{ORD},13} = \overline{G}^*_{s_{13}} \quad (31c)$$

$$\Delta\overline{G}^0_{\text{ORD},2} = \overline{G}^*_{s_2} \quad (31d)$$

$$\text{W}_{13} = -{}^{12}\!/_{49}\,\overline{G}^*_{r,s_{13}} + {}^{2}\!/_{7}\,\overline{G}^*_{r,s_{13}} - {}^{1}\!/_{3}\,\overline{G}^*_{s_{13},s_{13}} \quad (31e)$$

$$\text{W}_2 = -{}^{8}\!/_{49}\,\overline{G}^*_{r,s_2} + {}^{2}\!/_{7}\,\overline{G}^*_{r,s_2} - {}^{1}\!/_{2}\,\overline{G}^*_{s_2,s_2} \quad (31f)$$

$$\text{W}_4 = -{}^{8}\!/_{49}\,\overline{G}^*_{r,r} - {}^{2}\!/_{7}(\overline{G}^*_{r,s_{13}} + \overline{G}^*_{r,s_2}) - {}^{1}\!/_{2}(\overline{G}^*_{s_{13},s_{13}} + \overline{G}^*_{s_{13},s_2} + \overline{G}^*_{s_2,s_2}) \quad (31g)$$

$$\Delta\overline{G}^0_{X,123,4} = -{}^{80}\!/_{49}\,\overline{G}^*_{r,r} - {}^{6}\!/_{7}(\overline{G}^*_{r,s_{13}} + \overline{G}^*_{r,s_2}) + 2(\overline{G}^*_{s_{13},s_{13}} + \overline{G}^*_{s_{13},s_2} + \overline{G}^*_{s_2,s_2}) \quad (31h)$$

$$\Delta\overline{G}^0_{X,13,24} = -{}^{96}\!/_{49}\,\overline{G}^*_{r,r} + {}^{2}\!/_{7}\,\overline{G}^*_{r,s_{13}} + 2\overline{G}^*_{s_{13},s_{13}} \quad (31i)$$

$$\Delta\overline{G}^0_{X,134,2} = -{}^{80}\!/_{49}\,\overline{G}^*_{r,r} + {}^{6}\!/_{7}\,\overline{G}^*_{r,s_2} + 2\overline{G}^*_{s_2,s_2}. \quad (31j)$$

Note that the Taylor expansion coefficents $\overline{G}^*_0$, $\overline{G}^*_r$, and $\overline{G}^*_{r,r}$ do not appear in the expressions (Eq. 30) of homogeneous equilibrium. $\overline{G}^*_0$ and $\overline{G}^*_r$ must be calibrated from independent data on standard-state properties (Eqs. 31a and 31b). The coefficient $\overline{G}^*_{r,r}$ must be obtained from other data such as phase equilibrium constraints, as it represents an effective macroscopic regular-solution parameter (W):

$$\begin{aligned}(1-X)\overline{G}^0_{\text{Cm}} + X\overline{G}^0_{\text{Gn}} + (1-X)X\text{W} &= \left(\frac{1-r}{2}\right)\overline{G}^0_{\text{Cm}} + \left(\frac{1+r}{2}\right)\overline{G}^0_{\text{Gn}} + \left(\frac{1-r^2}{4}\right)\text{W} \\ &= \overline{G}^*_0 + \overline{G}^*_r r + \overline{G}^*_{r,r} r^2. \end{aligned} \quad (32)$$

Hence, $\overline{G}^*_{r,r} = -4\text{W}$. The analysis of the cation-ordering constraints consequently proceeds logically through a calibration of the seven Taylor coefficients of Equation 30. Then, subsequent calibration of $\overline{G}^*_{r,r}$ and adoption of standard-state properties yields, through Equation 31, all ten preferred model parameters.

The coefficients in Equation 30 may be calibrated by nonlinear regression analysis of the data plotted in Figure 1. For each datum we construct a residual function corresponding to predicted (via Eq. 30) minus measured values of the mole fraction of Fe on each site and minimize the sum of the squares of these residuals,

$$\text{SS} = \sum_{i=1}^{n} [(\hat{X}^{\text{M13}}_{\text{Fe},i} - X^{\text{M13}}_{\text{Fe},i})^2 + (\hat{X}^{\text{M2}}_{\text{Fe},i} - X^{\text{M2}}_{\text{Fe},i})^2 + (\hat{X}^{\text{M4}}_{\text{Fe},i} - X^{\text{M4}}_{\text{Fe},i})^2] \quad (33)$$

by nonlinear optimization (Marquardt's method, Nash, 1990). Optimal values, standard errors on these values, and correlations induced by the dataset are summarized in Table 8.

In Figure 1 we plot predicted isotherms calculated from the coefficients of Table 8. The somewhat pronounced temperature dependence of the ordering isotherms may seem at first mysterious in light of the fact that the fitted Taylor coefficients are temperature independent. This temperature dependence arises from the entropy term in Equation 30. In Figure 2 we graph the calculated entropy of mixing. These curves are completely determined by our fit of the cation-ordering data; the calculations do not depend on any adopted value of $\overline{G}^*_{r,r}$. The 0 K and ∞ K curves, i.e., the lowermost curve depicting entropy variation in the fully ordered state and the uppermost curve denoting the mixing entropy in the randomly ordered state, are model independent. Our model-dependent curves must interpolate between these two reference states, hence the pronounced increase in M2-M13 ordering at

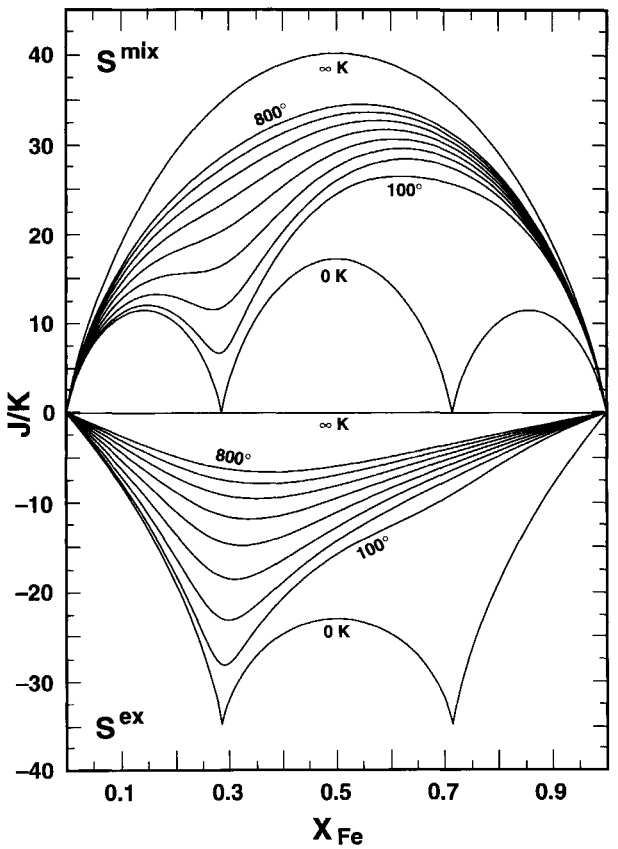

Fig. 2. Entropy of mixing and excess entropy of Fe-Mg cummingtonite computed from XRD ordering data and the three-site solution model proposed here. Note that the entropy of mixing is a strong asymmetric function of both composition and temperature. This renders modeling of the excess entropy utilizing a Margules approach highly problematic. The limiting curve for low temperature is calculated on the assumption that the M1 and M3 sites remain equivalent down to absolute zero.

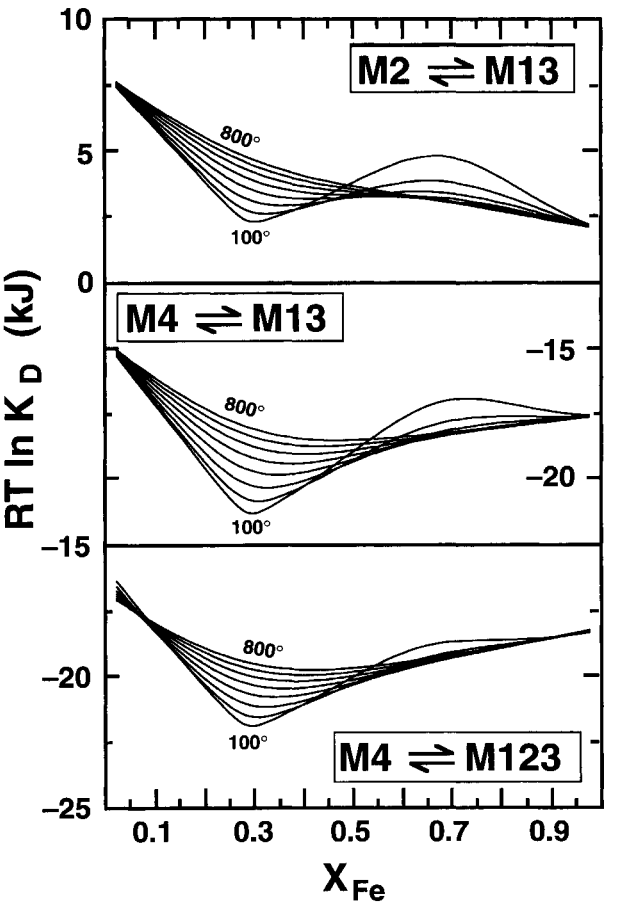

Fig. 3. Variation in intracrystalline partition coefficient as a function of macroscopic X_{Fe} of cummingtonite.

low temperatures is demanded by the theoretical value of the third law entropy and is not an arbitrary extrapolation from the high-temperature measurements.

In Figure 3 we plot $RT \ln K_D [K_D = (X^i_{Fe} X^i_{Mg})/(X^i_{Fe} X^i_{Mg})]$ corresponding to the simple Fe-Mg exchange reaction between the various crystallographic sites. These plots illustrate with high sensitivity the dependence of readily measured quantities on temperature and composition, and therefore serve as a guide to the collection of quality cation-ordering data, whether by X-ray (e.g., Hirschmann et al., 1994; Yang and Ghose, 1994), Mössbauer, or other techniques. Note that even at 800 °C values of K_D between sites are not independent of composition. Furthermore, the convergence of K_D values at the extremes of composition required by our model is something that goes undetected by the measurements, since uncertainties in site population ratios tend to infinity as X_{Fe} or X_{Mg} approach zero.

Phase equilibrium constraints

In order to complete the calibration of our model, we need to examine phase equilibrium constraints involving cummingtonite and at least one other ferromagnesian phase. Fortunately, the wealth of experimental data obtained by Fonarev and coworkers (Fonarev et al., 1976, 1979; Fonarev and Korolkov, 1980; Fonarev, 1987) affords an excellent basis for completing the calibration and testing the consequences of the derived model.

Fonarev and Korolkov (1980) provide half-brackets on the two-phase loop between Fe^{2+}-Mg orthopyroxene and cummingtonite solid solutions. We plot their data in Figure 4. These reversals may be used to estimate $\overline{G}^*_{r,r}$ provided we accept the standard-state values and ordering calibration discussed above and adopt an internally consistent model for the mixing properties of Fe-Mg orthopyroxenes. Sack and Ghiorso's (1989) solution model meets this criterion, in that it is consistent with the standard-state database of Berman (1988). We estimate an optimal value of $\overline{G}^*_{r,r}$ by calculating two-phase loops (drawn as the solid curves in Figure 4) and comparing

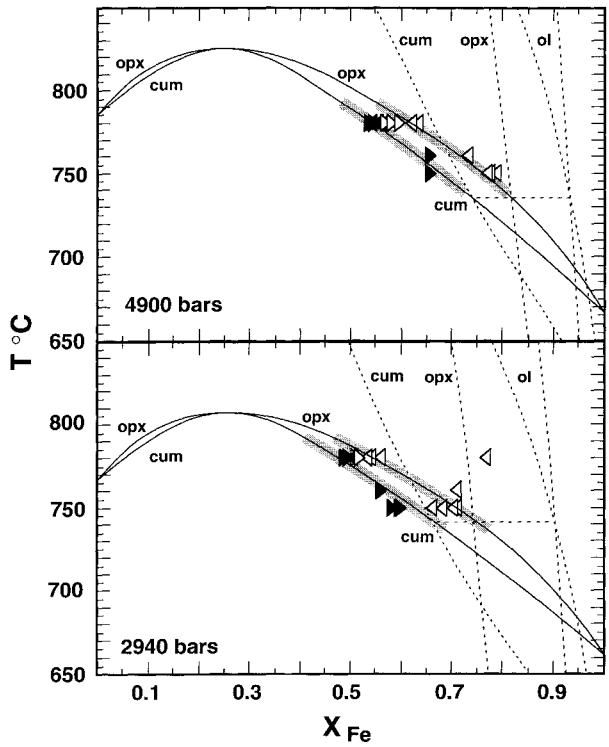

Fig. 4. Half-brackets on the compositions of cummingtonite (solid triangles) and orthopyroxene (open triangles) in the assemblage cummingtonite + orthopyroxene + quartz + H_2O from experiments at 2940 and 4900 bars by Fonarev and Korolkov (1980). Triangles point in the direction of change during the experiment. Solid curves: cum + opx phase-loop (metastable at low temperatures) fit to the experiments by adjustment of $\overline{G}^*_{r,r}$ (see text). The shaded curve denotes a variation of ±0.5 kJ in $\overline{G}^*_{r,r}$. Dashed curves: calculated phase-loops for cum + ol and opx + ol, in part metastable (see Fig. 8). The two-phase loop calculated at 2 kbar fits all the phase increase/decrease constraints determined experimentally for the composition $X_{Fe} = 0.5$ by Cameron (1975).

them visually to the reversals of Fonarev and Korolkov (1980). Equilibrium solutions (T, X^{Cum}_{Fe}, and X^{Opx}_{Fe}) are obtained by solving simultaneously mass action expressions corresponding to the following reactions:

$$\underset{\text{Cum}}{Fe_7Si_8O_{22}(OH)_2} = \underset{\text{Opx}}{7FeSiO_3} + \underset{\text{Qtz}}{SiO_2} + \underset{\text{vapor}}{H_2O} \quad (34)$$

$$\underset{\text{Cum}}{Fe_7Si_8O_{22}(OH)_2} + \underset{\text{Opx}}{7MgSiO_3} = \underset{\text{Cum}}{Mg_7Si_8O_{22}(OH)_2} + \underset{\text{Opx}}{7FeSiO_3}. \quad (35)$$

An optimal value of −11.2 kJ leads to the curves shown in Figure 4. By application of Equations 31c–31j this leads to values of the preferred model parameters reported in Table 9. Standard-error estimates on these values are calculated from the error estimates and correlation parameters reported in Table 8 for the Taylor expansion coefficients and an assumed standard error on $\overline{G}^*_{r,r}$ of zero. Consequently, these error estimates reflect uncertainties in fitting the cation-ordering data and not those of the experimental brackets. Acceptable fits to the reversal brackets shown in Figure 4 can be achieved for values of $\overline{G}^*_{r,r}$ ranging from −11.4 to −11.0. This additional level of uncertainty will propagate to the preferred values of W_4 (Eq. 31g), $\Delta\overline{G}^0_{X,123,4}$ (Eq. 31h), $\Delta\overline{G}^0_{X,13,24}$ (Eq. 31i), and $\Delta\overline{G}^0_{X,134,2}$ (Eq. 31j).

TABLE 9. Values of model parameters

Parameter	Value (kJ)	Standard error (kJ)
W_1	n.d.	n.d.
W_2	4.324	1.668
W_3	n.d.	n.d.
W_4	3.560	0.425
W_{13}	4.592*	1.458*
W_{123}	5.116*	0.171*
$\Delta\overline{G}^0_{X,123,4}$	12.103	1.486
$\Delta\overline{G}^0_{X,124,3}$	n.d.	n.d.
$\Delta\overline{G}^0_{X,134,2}$	15.113	5.611
$\Delta\overline{G}^0_{X,234,1}$	n.d.	n.d.
$\Delta\overline{G}^0_{X,12,34}$	n.d.	n.d.
$\Delta\overline{G}^0_{X,13,24}$	3.296	10.374
$\Delta\overline{G}^0_{X,23,14}$	n.d.	n.d.
$\Delta\overline{G}^0_{X,14,23}$	n.d.	n.d.
$\Delta\overline{G}^0_{ORD,1}$	n.d.	n.d.
$\Delta\overline{G}^0_{ORD,2}$	−16.248	0.998
$\Delta\overline{G}^0_{ORD,3}$	n.d.	n.d.
$\Delta\overline{G}^0_{ORD,13}$	−9.608*	0.803*
$\Delta\overline{G}^0_{ORD,123}$	−25.856*	0.820*
$\Delta\overline{G}^0_{\Delta ORD}$	5.905*	4.973*
$\Delta\overline{G}^0_{\Delta\Delta ORD}$	n.d.	n.d.

Note: n.d. = not determined.
* Parameter specific to the three- or two-site model.

Our calibration may be tested by comparing predicted curves to reversal brackets on other cummingtonite-bearing reactions investigated experimentally by Fonarev and coworkers. In Figure 5 we plot data obtained by Fonarev et al. (1976) and Fonarev (1987) on the breakdown of cummingtonite to magnetite + quartz + H_2O at 4.9 kbars and at f_{O_2} defined by the nickel + nickel oxide (NNO) buffer. The plotted curve corresponds to simultaneous solution of the equilibria

$$\underset{\text{Cum}}{Fe_7Si_8O_{22}(OH)_2} + \tfrac{7}{6}O_2 = \underset{\text{Mag}}{\tfrac{7}{3}Fe_3O_4} + \underset{\text{Qtz}}{8SiO_2} + \underset{\text{vapor}}{H_2O} \quad (36)$$

and

$$\underset{\text{Cum}}{Fe_7Si_8O_{22}(OH)_2} + \underset{\text{Mag}}{7MgFe_2O_4} = \underset{\text{Mag}}{7Fe_3O_4} + \underset{\text{Cum}}{Mg_7Si_8O_{22}(OH)_2}. \quad (37)$$

The magnetite limb of the loop plots essentially at pure Fe_3O_4. We utilize standard-state data for magnetite, quartz, O_2, and H_2O from Berman (1988) and the internally consistent thermodynamic model of Sack and

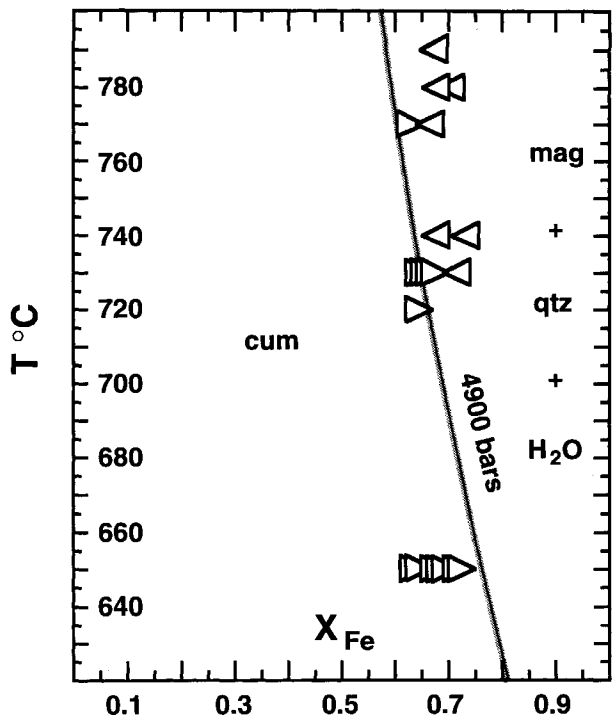

Fig. 5. Comparison of model T-X_{Fe} equilibrium curve at 4900 bars (NNO buffer) for the redox assemblage cummingtonite + magnetite + quartz + H_2O with half-brackets determined in experiments by Fonarev et al. (1976), as revised by Fonarev (1987). Omitted: experiments of ½- and 1-d duration, and experiments where X_{Fe} of cummingtonite changed by 1% or less. The shaded curve denotes a variation of ±0.5 kJ in $\overline{G}^*_{r,r}$.

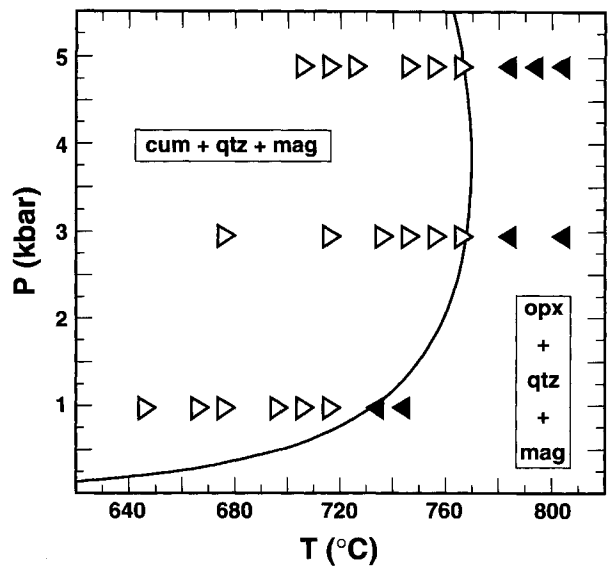

Fig. 6. Comparison of model P-T equilibrium curve (NNO buffer) for the assemblage cummingtonite + orthopyroxene + quartz + magnetite + H_2O with experimental half-brackets by Fonarev (1987). Open triangles: decrease or loss of opx; solid triangles: decrease or loss of cum.

Ghiorso (1991a) for the spinel. Agreement between the calculated curve and the half-brackets is within the limits of experimental error. In Figure 6 we examine the breakdown of cummingtonite to orthopyroxene in the presence of magnetite + quartz (Fonarev, 1987). The f_{O_2} was controlled by the NNO buffer, the compositions of cummingtonite and orthopyroxene being free to adjust to the imposed f_{O_2}. The calculated curve is obtained by simultaneous solution of mass action expressions corresponding to Reactions 34, 35, 36, and 37. As in Figure 5, the calculated magnetite composition is essentially pure Fe_3O_4. In addition to noting the excellent agreement between measured brackets and the calculated curve, it should be observed that our calibration predicts a maximum in temperature for the stability field of cummingtonite on the NNO buffer corresponding to about 4 kbar pressure.

Experimental data of Fonarev and Korolkov (1980) provide constraints on the stability of cummingtonite with respect to breakdown to Fe-Mg olivine and orthopyroxene. In Figure 7 we plot reversal brackets on the univariant four-phase assemblage cummingtonite + olivine + orthopyroxene + quartz and compare them to the calculated curve obtained by solving simultaneously mass action expressions consistent with Reactions 34, 35,

$$\underset{\text{Cum}}{Fe_7Si_8O_{22}(OH)_2} = \tfrac{7}{2}\underset{\text{Ol}}{Fe_2SiO_4} + \tfrac{7}{2}\underset{\text{Qtz}}{SiO_2} + \underset{\text{vapor}}{H_2O} \quad (38)$$

and

$$\underset{\text{Cum}}{Fe_7Si_8O_{22}(OH)_2} + \tfrac{7}{2}\underset{\text{Ol}}{Mg_2SiO_4} = \underset{\text{Cum}}{Mg_7Si_8O_{22}(OH)_2} + \tfrac{7}{2}\underset{\text{Ol}}{Fe_2SiO_4}. \quad (39)$$

Standard-state data for olivines are from Berman (1988) and the mixing properties of olivine are taken from Sack and Ghiorso (1989). Above 3 kbar we predict a negative dP/dT slope for the four-phase assemblage. A positive dP/dT slope (Fonarev and Korolkov, 1980) is also possible for this assemblage, considering the experimental data in Figures 4 and 7 alone.

In Figure 8, half-brackets on the cummingtonite-olivine loop (Fonarev et al., 1979) are plotted at two pressures, and calculated curves are obtained by simultaneous solution of mass action expressions corresponding to Reactions 38 and 39. The agreements demonstrated in Figures 7 and 8 are good and support the olivine mixing model proposed by Sack and Ghiorso (1989). This model has recently been called into question by Wiser and Wood (1991) and von Seckendorff and O'Neill (1993). On the basis of high-temperature experimental work involving Fe-Mg exchange between magnesiowüstite and olivine and between orthopyroxene and olivine, respectively, these authors deduce a much smaller degree of nonideality in Fe-Mg olivine solid solutions than that proposed by Sack and Ghiorso (1989), who based their analysis on phase

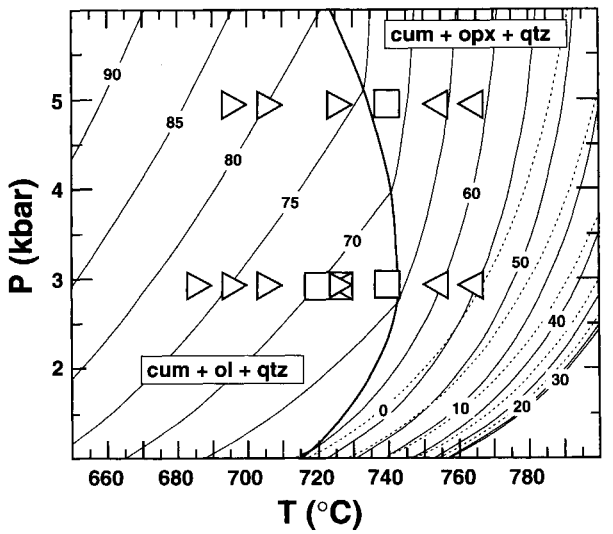

Fig. 7. Comparison of model P-T equilibrium curve for the assemblage cummingtonite + olivine + orthopyroxene + quartz + H_2O with experimental half-brackets determined by Fonarev and Korolkov (1980). Right-pointing triangles: loss of opx; left-pointing triangles: loss of cum; squares: no change. Isopleths are for percent grunerite in cummingtonite.

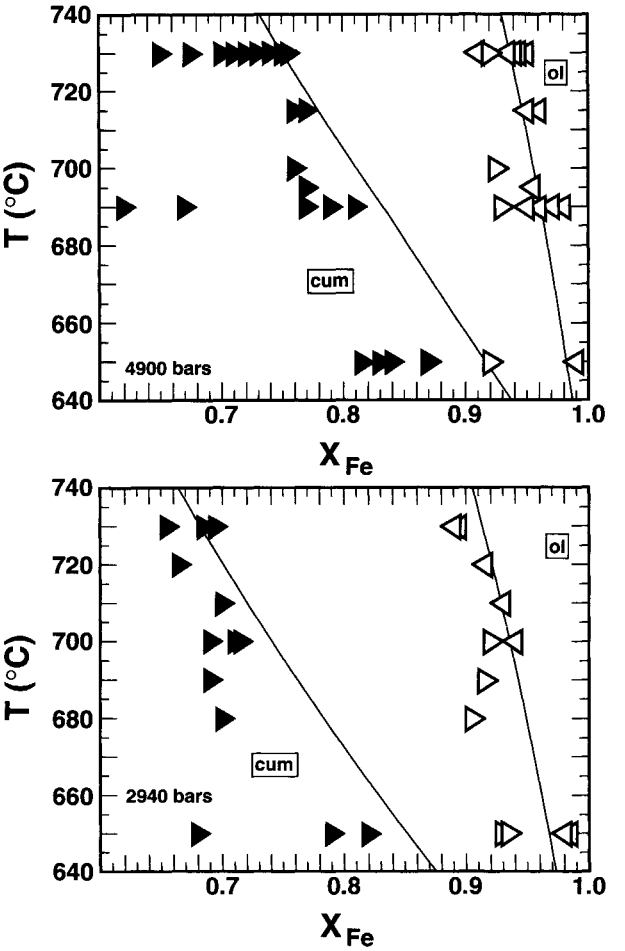

Fig. 8. Comparison of model T-X_{Fe} equilibrium curves at 2940 and 4900 bars for the assemblage cummingtonite + olivine + quartz + H_2O with experimental half-brackets by Fonarev et al. (1979). Triangles point in the direction of change during the experiment. Experiments with $<1\%$ change in X_{Fe} omitted.

relations between orthopyroxene and olivine, direct determinations of the activity of fayalite in olivine, and enthalpy of solution data on olivine solid solutions. The conclusions of Wiser and Wood (1991) and von Seckendorff and O'Neill (1993) are inconsistent with the experimental data displayed in Figures 7 and 8 when these data are analyzed in conjunction with Berman (1988) and the cummingtonite solution model presented here. A significantly more ideal olivine shifts the calculated curve in Figure 7 to the right, and for Wiser and Wood's (1991) value, the curve is shifted to a maximum temperature of 780 °C. Sack and Ghiorso's (1989) analysis of the likely degree of nonideality in Fe-Mg olivine is further supported by the recent discovery of exsolution in ferromagnesian olivine (Petaev and Brearley, 1994) and by the observation that the cummingtonite solution model presented here is not entirely dependent upon that of orthopyroxene (and therefore circularly upon the olivine model of Sack and Ghiorso, 1989). Sack and Ghiorso (1991c) calibrate macroscopic thermodynamic mixing models for cummingtonite and olivine that are based solely on Fe-Mg distribution between natural olivine + cummingtonite pairs. Their analysis yields an olivine interaction parameter that is consistent with Sack and Ghiorso (1989) and a degree of nonideality in cummingtonite nearly identical to that proposed here. Additionally, the degree of nonideality attributed to orthopyroxene by Sack and Ghiorso (1989) has been verified recently by Yang and Ghose (1994), who base their analysis on high-quality Fe-Mg cation-ordering data in orthopyroxene, independent of olivine and cummingtonite. Finally, the cummingtonte model proposed here gives a consistent calibration of the phase reversals plotted in Figure 5, which depends only upon the standard-state properties of magnetite, quartz, O_2, and H_2O (Berman, 1988). All this corroborative evidence suggests that Sack and Ghiorso's (1989) original conclusion with regard to the nonideality of the thermodynamic mixing properties in Fe-Mg olivine, at least in the range 600–800 °C, is strongly supported by our analysis of phase equilibria involving cummingtonite. However, it should be borne in mind that the mixing properties of cummingtonite, olivine, and orthopyroxene adopted in this paper represent one of a family of sets of internally consistent models, and their mutual consistency in conjunction with the standard-state database of Berman (1988) does not imply that they uniquely constrain the thermodynamic properties of this system.

As a final test of our calibration, we have collected data from the literature on compositions of coexisting olivine + cummingtonite and orthopyroxene + cummingtonite solid solutions found in natural parageneses. These data

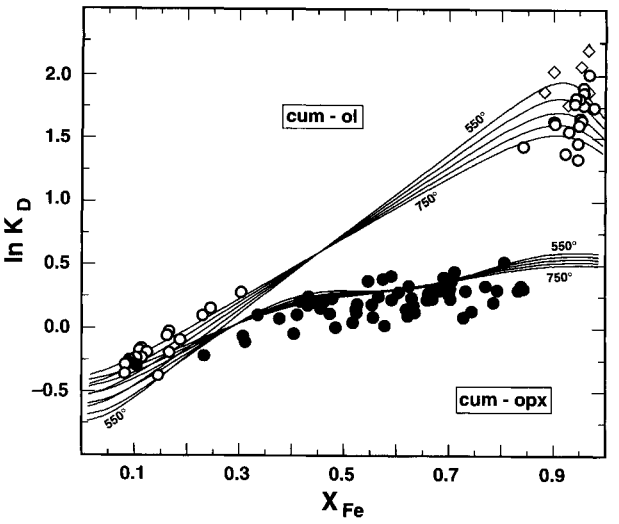

Fig. 9. Model isotherms for intercrystalline partitioning of Mg and Fe between cummingtonite and olivine and cummingtonite and orthopyroxene compared to data compiled from the literature. X_{Fe} (x axis) is composition of olivine and orthopyroxene, respectively. Open circles: ol-cum pairs, with probable equilibration temperatures in the range 575–725 °C; diamonds indicate Mn-rich samples. Solid circles: opx-cum pairs, with probable equilibration temperatures in the range 625–780 °C.

are illustrated in Figure 9 in terms of a macroscopic K_D for Fe^{2+}-Mg^{2+} exchange [e.g., $K_D^{Ol} = (X_{Fe}^{Ol} X_{Mg}^{Cum})/(X_{Fe}^{Cum} - X_{Mg}^{Ol})$] plotted against the Fe content of the olivine or orthopyroxene. Adopting the thermodynamic formulation of Sack and Ghiorso (1989) for the olivines and orthopyroxenes, we obtain the model calibration indicated in the figure by evaluating mass action expressions corresponding to Reactions 35 and 39. In light of uncertainties inherent in projecting mineral compositions, the difficulty of estimating equilibrium temperatures of natural assemblages, and the likely existence of exchange disequilibrium in natural pairs, the agreement shown in Figure 9 is excellent. Note in particular the reversal in partitioning (at $\ln K_D = 0$) between Fe- and Mg-rich bulk compositions, already seen as the extremum in Figure 4.

Applications

In a future contribution (Evans and Ghiorso, 1995), we will present a number of applications that bear on cummingtonite stability relations in metamorphic and silicic volcanic rocks. We end this paper with three generic applications that focus on some thermodynamic consequences of the model calibration. In Figure 10, the Gibbs free energy of mixing, the excess Gibbs free energy, and the enthalpy of mixing of Fe-Mg cummingtonite solid solutions are plotted as functions of composition and temperature. The Gibbs free energy of mixing is given by

$$\overline{G}_{mix} = \overline{G} - X_{Fe}\,\overline{G}_{Gn} - (1 - X_{Fe})\overline{G}_{Cm} \qquad (40)$$

(where $\overline{G}$ is provided by Eq. T5-1), the enthalpy of mixing by

$$\overline{H}_{mix} = \overline{G}_{mix} + T\overline{S}_{conf} \qquad (41)$$

and the excess Gibbs free energy by

$$\overline{G}_{ex} = \overline{G}_{mix} - 7RT(X_{Fe}\ln X_{Fe} + X_{Mg}\ln X_{Mg}). \qquad (42)$$

The quantity subtracted from $\overline{G}_{mix}$ on the right side of Equation 42 is the macroscopic Gibbs free energy of mixing of a seven-site ideal solution. The temperature dependence of the curves shown in Figure 10 arises from the configurational entropy term and reflects variation in the degree of cation ordering as a function of temperature. This is easily seen by writing out the molar Gibbs energy of mixing in terms of its configurational ($-T\overline{S}_{conf}$) and nonconfigurational components ($\overline{G}^*_{mix}$; just $\overline{G}^*$ minus the standard-state terms):

$$\overline{G}_{mix} = -T\overline{S}_{conf} + \overline{G}^*_{mix}. \qquad (43)$$

Taking the temperature derivative of Equation 43 we obtain the molar entropy of mixing, recognizing that $\overline{G}^*_{mix}$ is modeled as temperature independent, i.e., in calibrating our model we assume that there is no vibrational component to the entropy of mixing:

$$\frac{\partial \overline{G}_{mix}}{\partial T} = -\overline{S}_{mix} = -\overline{S}_{conf} - T\frac{\partial \overline{S}_{conf}}{\partial T}. \qquad (44)$$

Combining this result with Equation 43 yields an expression for the molar enthalpy of mixing:

$$\overline{H}_{mix} = \overline{G}_{mix} + T\overline{S}_{mix} = \overline{G}^*_{mix} - T\frac{\partial \overline{S}_{conf}}{\partial T}. \qquad (45)$$

Equations 43 and 45 clearly demonstrate that the temperature dependence of $\overline{G}_{mix}$ and $\overline{H}_{mix}$ is a consequence of that in $\overline{S}_{conf}$. Note in Figure 10 how the Gibbs energy of mixing becomes more symmetrical at elevated temperature as the degree of cation ordering diminishes. Additionally, note the pronounced minima in the calculated low-temperature curves for $\overline{G}_{ex}$ and $\overline{H}_{mix}$. This is mainly a consequence of the large ordering energy ($\Delta\overline{G}^0_{ORD,123} = \Delta\overline{G}^0_{ORD,1} + \Delta\overline{G}^0_{ORD,2} + \Delta\overline{G}^0_{ORD,3}$, see Table 9), which stabilizes Fe on the M4 site in strong preference to the M13 or M2. As the temperature decreases, the configurational entropy tends to zero at the composition corresponding to the ordered compound $Fe_2^{M4}Mg^{M1}Mg_2^{M2}Mg^{M3}Si_8O_{22}(OH)_2$ (i.e., $X_{Fe} = 2/7$, $r = -3/7$, $X_{Fe}^{M4} = 1$, $X_{Fe}^{M13} = 0$, $X_{Fe}^{M2} = 0$), and this results in a molar Gibbs energy of mixing given by

$$\begin{aligned}\overline{G}_{mix}\,|_{T\to 0, r=-3/7} &= \Delta\overline{G}^0_{ORD,1} + \Delta\overline{G}^0_{ORD,2} + \Delta\overline{G}^0_{ORD,3} \\ &\quad + \tfrac{1}{2}\Delta\overline{G}^0_{123,4} \\ &= \Delta\overline{G}^0_{ORD,123} + \tfrac{1}{2}\Delta\overline{G}^0_{X,123,4} \end{aligned} \qquad (46)$$

which may be derived from the three-site expression for $\overline{G}$ in Table 5. As the temperature increases, less Fe orders onto the M4 site, and the energetic contribution owing to this stabilization is overwhelmed by the configurational energy of the more random cation distribution. We predict

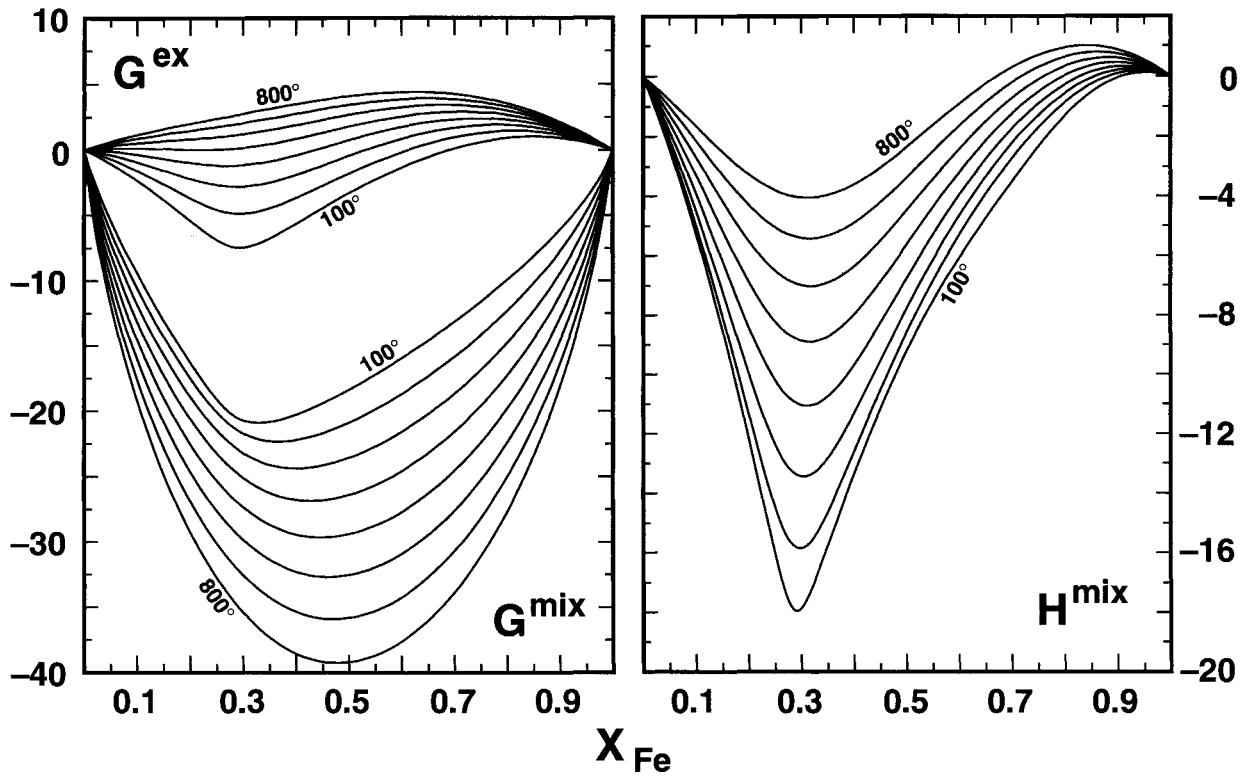

Fig. 10. Calculated Gibbs energy of mixing, excess Gibbs energy of mixing, and enthalpy of mixing of Fe-Mg cummingtonite.

that determinations of enthalpy of mixing in cummingtonite solid solutions should show both positive and negative deviations from ideality as a function of composition (Fig. 10).

In Figure 11 we plot calculated activity-composition relations as a function of composition and temperature. The complex behavior of the isotherms is a consequence of the temperature- and composition-dependent cation ordering. Fonarev (1981, 1987) constructed activity-composition relations of cummingtonite using a macroscopic formulation and a series of phase equilibrium experiments (in the range 600–800 °C) involving olivine, orthopyroxene, quartz, and magnetite. Above 750 °C, our results do not differ greatly from his, but at progressively lower temperatures the differences become large. This discrepancy is due largely to the inability of Fonarev's (1981) model to extrapolate correctly from the ordering states that characterize his experimentally equilibrated cummingtonite to the significantly different ordering conditions that develop at lower temperatures. Fonarev's (1981) model proxies a macroscopic ideal entropy of mixing combined with a temperature-dependent excess entropy of mixing for the configurational entropy of disorder. Consequently, the functional form of his modeled entropy of mixing does not incorporate the correct low-temperature limiting behavior as displayed in Figure 2. This failure results in increasingly more pronounced differences between our model results (Fig. 11) and those of Fonarev as temperature is progressively lowered.

Our calculated 700 °C isotherm is consistent with the experimentally determined values for orthoamphibole in Popp et al. (1977). It should be noted that, at elevated temperatures and Mg-rich compositions, the activity-

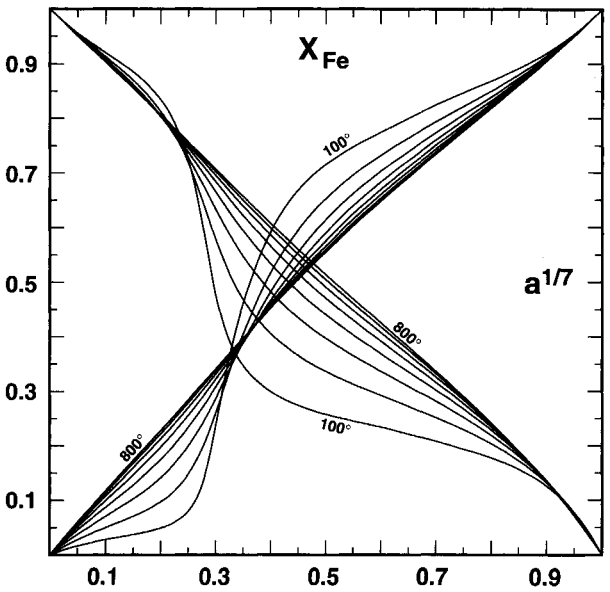

Fig. 11. Activity-composition relations for Mg- and Fe-end-members of cummingtonite. Note that activities are referenced to a one-site basis.

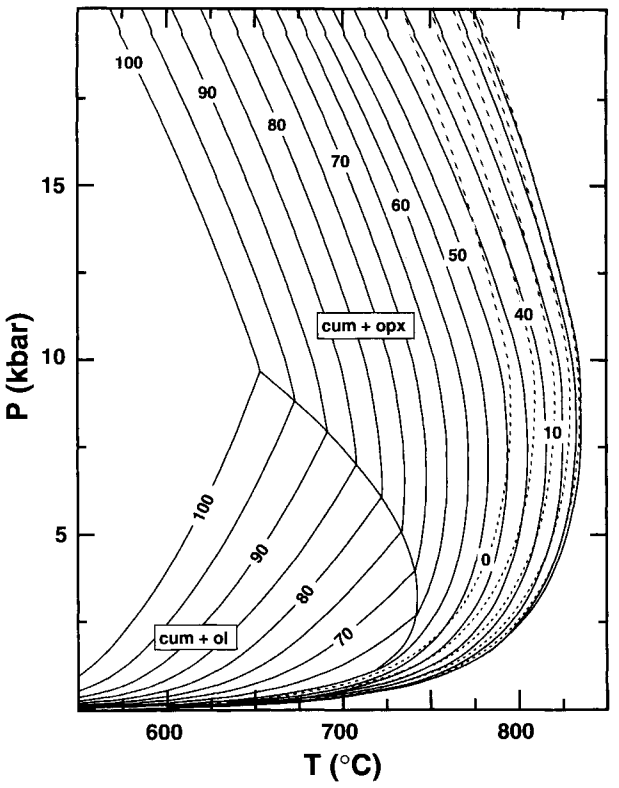

Fig. 12. P-T phase diagram showing the calculated stability limit of Fe-Mg cummingtonite (as isopleths of X_{Fe} in cummingtonite) with respect to quartz, H_2O, and orthopyroxene (at high P and T) and olivine (at low P and T). Dashed lines are isopleths in the magnesio-cummingtonite range. At high P and T cummingtonite is metastable with respect to talc + orthopyroxene.

composition relations for $Mg_7Si_8O_{22}(OH)_2$ closely approach those of ideal mixing.

As a final application, we have constructed (Fig. 12) a P-T stability diagram at quartz saturation for the system FeO-MgO-SiO_2-H_2O with fields for Fe-Mg cummingtonite, olivine, and orthopyroxene. Contours denote mole percent grunerite in the cummingtonite. The P-T curve of the four-phase assemblage (cummingtonite + orthopyroxene + olivine + quartz) has a temperature maximum at about 3 kbar (see enlargement in Fig. 7). The maximum stability limit of cummingtonite at quartz saturation (with breakdown to orthopyroxene) occurs at about 8 kbar and 830 °C for an approximate composition of 25 mol% grunerite end-member. Although it might be tempting to attribute this extremum to the same stabilization energy that generates the minima in $\overline{G}_{ex}$ and $\overline{H}_{mix}$ of Figure 10, the correspondence is fortuitous. The temperature extremum at X_{Fe} of ~0.25 results from a combination of standard-state and solution properties of both cummingtonite and orthopyroxene. The extremum composition actually shifts from ~0.30 at 1 kbar to ~0.20 at 20 kbar. A metastable extremum involving cummingtonite and olivine occurs, if at all, at very high temperature with $X_{Fe}^{Cum} < 0.2$. Our calculations demonstrate that olivine and cummingtonite coexist over a restricted range of P-T conditions and that the maximum temperature of coexistence (740 °C) virtually precludes this phenocryst assemblage from occurring in silicic volcanic rocks (unless stabilization by Al, Fe^{3+}, and Ca is significant).

Acknowledgments

We would like to thank L. Aranovich, R.G. Berman, P. Davidson, and T. Will for helpful reviews and R.G. Berman for providing revised, internally consistent, thermodynamic data on anthophyllite. Material support for this investigation was provided by the National Science Foundation through grants EAR-9104714 and EAR-9303972. Computations were facilitated by a generous equipment grant from Digital Equipment Corporation.

References cited

Anovitz, L.M., Essene, E.J., Hemingway, B.S., Komada, N.L., and Westrum, E.F., Jr. (1988) The heat capacities of grunerite and deerite: Phase equilibria in the system Fe-Si-C-O-H and implications for the metamorphism of banded iron formations. Eos, 69(16), 515.

Bancroft, G.M., Burns, R.G., and Maddock, A.G. (1967) Determination of cation distribution in the cummingtonite-grunerite series by Mössbauer spectra. American Mineralogist, 52, 1009–1026.

Barabanov, A.V., and Tomilov, S.B. (1973) Mössbauer study of the isomorphous series anthophyllite-gedrite and cummingtonite-grunerite. Geochemistry International, 10, 1240–1247.

Berman, R.G. (1988) Internally-consistent thermodynamic data for minerals in the system Na_2O-K_2O-CaO-MgO-FeO-Fe_2O_3-Al_2O_3-SiO_2-TiO_2-H_2O-CO_2. Journal of Petrology, 29, 445–522.

Cameron, K.L. (1975) An experimental study of actinolite-cummingtonite phase relations with notes on the synthesis of Fe-rich anthophyllite. American Mineralogist, 60, 375–390.

Carpenter, M.A. (1982) Amphibole microstructures: Some analogies with phase transformations in pyroxenes. Mineralogical Magazine, 46, 395–397.

Chernosky, J.V., Jr., Day, H.W., and Caruso, L.J. (1985) Equilibria in the system MgO-SiO_2-H_2O: Experimental determination of the stability of Mg-anthophyllite. American Mineralogist, 70, 223–236.

Evans, B.W., and Ghiorso, M.S. (1995) Thermodynamics and petrology of cummingtonite. American Mineralogist, 80, in press.

Fonarev, V.I. (1981) Thermodynamic functions of cummingtonite solid solutions. Geochemistry International, 18(5), 1–11.

——— (1987) Mineral equilibria in the Precambrian iron formations, 294 p. Akademia Nauk, Moscow (in Russian).

Fonarev, V.I., and Korolkov, G.J. (1980) The assemblage orthopyroxene + cummingtonite + quartz: The low-temperature stability limit. Contributions to Mineralogy and Petrology, 73, 413–420.

Fonarev, V.I., Korolkov, G.J., and Dokina, T.N. (1976) Stability of the cummingtonite-quartz-magnetite association. Geochemistry International, 13, 34–45.

——— (1979) Laboratory data on the stability of the cummingtonite + olivine + quartz association. Geochemistry International, 16, 21–32.

Ganguly, J. (1982) Mg-Fe order-disorder in ferromagnesian silicates: II. Thermodynamics, kinetics and geological applications. In Advances in Physical Geochemistry, 2, 58–99.

Ghiorso, M.S. (1990a) Thermodynamic properties of hematite-ilmenite-geikielite solid solutions. Contributions to Mineralogy and Petrology, 104, 645–667.

——— (1990b) Application of the Darken equation to mineral solid solutions with variable degree of order-disorder. American Mineralogist, 75, 539–543.

Ghiorso, M.S., and Sack, R.O. (1991) Fe-Ti oxide geothermometry: Thermodynamic formulation and the estimation of intensive variables in silicic magmas. Contributions to Mineralogy and Petrology, 108, 485–510.

Ghose, S. (1981) Subsolidus reactions and microstructures in amphiboles. In Mineralogical Society of America Reviews in Mineralogy, 9A, 325–372.

Ghose, S., and Weidner, J.R. (1972) Mg^{2+}-Fe^{2+} order-disorder in cummingtonite, $(Mg,Fe)_7Si_8O_{22}(OH)_2$: A new geothermometer. Earth and Planetary Science Letters, 16, 346–354.

Greenwood, H.J. (1963) The synthesis and stability of anthophyllite. Journal of Petrology, 4, 317–351.

Hafner, S.S., and Ghose, S. (1971) Iron and magnesium distribution in cummingtonites, $(Fe,Mg)_7Si_8O_{22}(OH)_2$. Zeitschrift für Kristallographie, 133, 301–326.

Hawthorne, F.C. (1981) Crystal chemistry of the amphiboles. In Mineralogical Society of America Reviews in Mineralogy, 9A, 1–102.

——— (1983) The crystal chemistry of the amphiboles. Canadian Mineralogist, 21, 173–480.

Hemingway, B.S. (1991) Thermodynamic properties of anthophyllite and talc: Corrections and discussion of calorimetric data. American Mineralogist, 76, 1589–1596.

Hirschmann, M. (1991) Thermodynamics of multicomponent olivines and the solution properties of $(Ni,Mg,Fe)_2SiO_4$ and $(Ca,Mg,Fe)_2SiO_4$ olivines. American Mineralogist, 76, 1232–1248.

Hirschmann, M., Evans, B.W., and Yang, H. (1994) Composition and temperature dependence of Fe-Mg ordering in cummingtonite-grunerite as determined by X-ray diffraction. American Mineralogist, 79, 862–877.

Holland, T.J.B. (1989) Dependence of entropy on volume for silicate and oxide minerals: A review and predictive model. American Mineralogist, 74, 5–13.

Holland, T.J.B., and Powell, R. (1990) An enlarged and updated internally consistent thermodynamic dataset with uncertainties and correlations: The system K_2O-Na_2O-CaO-MgO-MnO-FeO-Fe_2O_3-Al_2O_3-TiO_2SiO_2-C-H_2-O_2. Journal of Metamorphic Geology, 8, 89–124.

Lattard, D., and Evans, B.W. (1992) New experiments on the stability of grunerite. European Journal of Mineralogy, 4, 219–238.

Law, A.D. (1989) Studies of the orthoamphiboles: IV. Mössbauer spectra of anthophyllites and gedrites. Mineralogical Magazine, 370, 181–192.

Lawson, A.W. (1947) On simple binary solid solutions. Journal of Chemical Physics, 15, 831–842.

Mueller, R.F. (1961) Analysis of relations among Mg, Fe, and Mn in certain metamorphic minerals. Geochimica et Cosmochimica Acta, 25, 267–296.

——— (1962) Energetics of certain silicate solutions. Geochimica et Cosmochimica Acta, 26, 581–598.

Nash, J.C. (1990) Compact numerical methods for computers (2nd edition), 278 p. Adam Hilger, New York.

Petaev, M.I., and Brearley, A.J. (1994) Exsolution in ferromagnesian olivine of the Divnoe meteorite. Science, 266, 1545–1547.

Popp, R.K., Gilbert, M.C., and Craig, J.R. (1977) Stability of Fe-Mg amphiboles with respect to sulfur fugacity. American Mineralogist, 62, 13–30.

Prewitt, C.T., Papike, J.J., and Ross, M. (1970) Cummingtonite: A reversible nonquenchable transition from $P2_1/m$ to $C2/m$ symmetry. Earth and Planetary Science Letters, 8, 448–450.

Ross, M., Papike, J.J., and Shaw, K.W. (1969) Exsolution textures in amphiboles as indicators of subsolidus thermal histories. Mineralogical Society of America Special Papers, 2, 275–299.

Sack, R.O., and Ghiorso, M.S. (1989) Importance of considerations of mixing properties in establishing an internally consistent database: Thermochemistry of minerals in the system Mg_2SiO_4-Fe_2SiO_4-SiO_2. Contributions to Mineralogy and Petrology, 102, 41–68.

——— (1991a) An internally consistent model for the thermodynamic properties of Fe-Mg-titanomagnetite-aluminate spinels. Contributions to Mineralogy and Petrology, 106, 474–505.

——— (1991b) Chromian spinels as petrogenetic indicators: Thermodynamics and petrological applications. American Mineralogist, 76, 827–847.

——— (1991c) Chromite as a petrogenetic indicator. In Mineralogical Society of America Reviews in Mineralogy, 25, 323–353.

——— (1994a) Thermodynamics of multicomponent pyroxenes: I. Formulation of a general model. Contributions to Mineralogy and Petrology, 116, 277–286.

——— (1994b) Thermodynamics of multicomponent pyroxenes: II. Applications to phase relations in the quadrilateral. Contributions to Mineralogy and Petrology, 116, 287–300.

——— (1994c) Thermodynamics of multicomponent pyroxenes: III. Calibration of $Fe^{2+}(Mg)_{-1}$, $TiAl_2(MgSi_2)_{-1}$, $TiFe^{3+}_2(MgSi_2)_{-1}$, $AlFe^{3+}(MgSi)_{-1}$, $NaAl(CaMg)_{-1}$, $Al_2(MgSi)_{-1}$ and $Ca(Mg)_{-1}$ exchange reactions between pyroxenes and silicate melts. Contributions to Mineralogy and Petrology, 118, 271–296.

Saxena, S.K. (1973) Thermodynamics of rock-forming crystalline solutions, 188 p. Springer-Verlag, New York.

Seifert, F. (1978) Equilibrium Mg-Fe^{2+} cation distribution in anthophyllite. American Journal of Science, 278, 1323–1333.

Seifert, F., and Virgo, D. (1974) Temperature dependence of intra-crystalline Fe^{2+}-Mg distribution in a natural anthophyllite. Carnegie Institution of Washington Year Book, 73, 405–411.

Thompson, J.B., Jr. (1969) Chemical reactions in crystals. American Mineralogist, 54, 341–375.

——— (1970) Chemical reactions in crystals: Corrections and clarification. American Mineralogist, 55, 528–532.

von Seckendorff, V., and O'Neill, H.St.C. (1993) An experimental study of Fe-Mg partitioning between olivine and orthopyroxene at 1173, 1273 and 1423 K and 1.6 GPa. Contributions to Mineralogy and Petrology, 113, 196–207.

Wiser, N.M., and Wood, B.J. (1991) Experimental determination of activities in Fe-Mg olivine at 1400 K. Contributions to Mineralogy and Petrology, 108, 146–153.

Yang, H., and Ghose, S. (1994) In-situ Fe-Mg order-disorder studies and thermodynamic properties of orthopyroxene $(Mg,Fe)_2Si_2O_6$. American Mineralogist, 79, 633–643.

Ying, Y., Li, Y., and Sun, C. (1989) Fe^{2+} site occupancy in cummingtonite and estimation of equilibrium temperature. Chinese Science Bulletin, 34, 1975–1979.

Zhang, L., Ahsbahs, H., Kutoglu, A., and Hafner, S.S. (1992) Compressibility of grunerite. American Mineralogist, 77, 480–483.

Manuscript received April 29, 1994
Manuscript accepted February 9, 1995